REPORT DOCUMENTATION PAGE	1. REPORT NO. NSF/RA-800207	2.	3. Recipient's Accession No. PB81 120032

4. Title and Subtitle
Nonlinear Hyperelastic (Green) Constitutive Models for Soils, Part I: Theory and Calibration; Part II: Predictions and Comparisons

5. Report Date
July 1980

6.

7. Author(s)
A. F. Saleeb, W. F. Chen

8. Performing Organization Rept. No.
CE-STR-80-9

9. Performing Organization Name and Address
Purdue University
School of Civil Engineering
West Lafayette, IN 47907

10. Project/Task/Work Unit No.

11. Contract(C) or Grant(G) No.
(C)
(G)PFR7809326

12. Sponsoring Organization Name and Address
Engineering and Applied Science (EAS)
National Science Foundation
1800 G Street, N.W.
Washington, D.C. 20550

13. Type of Report & Period Covered

14.

15. Supplementary Notes
Presented at the May 28-30, 1980 North American Workshop on Limit Equilibrium, Plasticity, and Generalized Stress-Strain in Geotechnical Engineering.

16. Abstract (Limit: 200 words)

Three formulation methods for elasticity based stress-strain relations for soils are reviewed. A non-linear hyperelastic constitutive model is described and applied to three types of soils--clays "X" and "Y" and Ottawa sand. A description of the procedure for determining the material constraints in the model has been made. Stress-strain relations for general straight line stress paths and for examples of stress paths in conventional soil tests are given. Incremental forms of constitutive relations, an approximate method of modeling unloading-reloading behavior, and a failure condition are included for general nonlinear finite element analyses. Major conclusions are: (1) The proposed constitutive relations can model many characteristics of soil behavior; (2) Present formulation satisfies mathematical requirements when used for monotonically increasing load conditions; (3) Incremental forms of the model can be implemented easily in finite element codes for general analyses; (4) For the cases studied, the model's results are in general agreement with experimental results; (5) The model behavior for Ottawa sand is sensitive to changes in values of material constants; (6) Best results from the model are generally expected at low stress levels below failure; and (7) The present formulation cannot account for post-failure in strain-softening materials.

17. Document Analysis a. Descriptors

Soil tests	Predictions	Stress analysis
Soil mechanics	Strain tests	Elastic analysis
Soil properties	Loads	Clay soils

b. Identifiers/Open-Ended Terms

Soil elasticity
Ottawa sand
Earthquake Hazards Mitigation

c. COSATI Field/Group

18. Availability Statement	19. Security Class (This Report)	21. No. of Pages
NTIS	20. Security Class (This Page)	22. Price

CE-STR-80-9 (1980)

NONLINEAR HYPERELASTIC (GREEN) CONSTITUTIVE MODELS FOR SOILS

PART I: THEORY AND CALIBRATION

PART II: PREDICTIONS AND COMPARISONS

by

A. F. Saleeb and W. F. Chen

Presented at the May 28-30, 1980, North American Workshop on Limit Equilibrium, Plasticity, and Generalized Stress-Strain in Geotechnical Engineering - Jointly Sponsored by NSF/NSERC.

This material is based upon work supported by the National Science Foundation under Grant No. PFR-7809326 to Purdue University.

July, 1980

List of Figures

Nonlinear Hyperelastic (Green) Constitutive Models for Soils: Theory and Calibration

By: A. F. Saleeb and W. F. Chen

School of Civil Engineering

Purdue University

West Lafayette, IN

1. Introduction

1.1 General

The stress-strain behavior of any type of soil subjected to externally applied loads is quite complicated and depends on many factors. This has been a subject of research for many years, and the advent of the numerical technique of finite element has given added impetus to these efforts [29]. The problems stem mainly from the fact that, unlike the properties of most engineering materials, soil stress-strain responses are greatly affected by such factors as soil structure (grain size, grain shape, surface texture, mineralogy, cementation or bonding, etc.), density, water content, drainage conditions, degree of voids saturation, loading rate, confining pressure, loading history, and current stress state [8, 11, 13, 30]. Clearly, the number of variables is far too extensive to offer any encouraging hope for developing a simple, yet realistic, constitutive relation that is capable of modelling the behavior of all soils under general loading conditions. Drastic idealizations and simplifications are essential in order to model mathematically and approximately the real behavior for the solution of the problem at hand. For example, in most of the presently available constitutive relations, soil behavior has been drastically idealized as time-independent, such as elastic and

elastic-plastic models where time effects are neglected. In addition, interaction between mechanical and thermal processes is usually neglected.

Recent work [6, 14, 18, 19, 21, 22] has indicated that the stress-strain behavior of most granular materials may be separated into recoverable and irrecoverable components, and attempts have been made to treat each component individually. The recoverable behavior is treated within the framework of elasticity theory; while the irrecoverable part is based on plasticity theory. Such separation is necessary if cyclic loading and unloading are encountered. However, for problems in which a monotonically increasing load prevails, elasticity based models provide a much simpler approach. Most of the commonly used plasticity models for soils are summarized in the recent paper by Chen [2]. In the forthcoming, three general methods of formulation for elasticity based stress-strain relations are reviewed. Later in this paper, a complete development of the proposed isotropic third-order hyperelastic model will be presented and its application to three different types of soils: clay "X", clay "Y" and Ottawa Sand will be discussed.

1.2 Review of Elasticity-Based Stress-Strain Relations

Three different types of elasticity-based constitutive models are presently available for general formulation. These are summarized in the following [4, 15]:

(1) Cauchy type in which the current state of stress depends only on the current state of deformation, i.e., stress is a function of strain. Mathematically, the constitutive equations for this material are given by:

$$\sigma_{ij} = F_{ij}(\varepsilon_{kl}) \tag{1}$$

where F_{ij} is the elastic response function of the material, σ_{ij} and ε_{kl} are the components of stress and strain tensors, respectively. The elastic behavior described by Eq. (1) is both reversible and path independent in the sense that stresses are uniquely determined from the current state of strain or vice versa. There is no dependence of the behavior on the stress or strain histories followed to reach the current state of stress or strain. It can be shown [4] that Cauchy elastic material may generate energy under certain loading-unloading cycles. Such behavior is inadmissible since it violates the laws of thermodyanmics. This leads naturally to the consideration of the second type of formulation, Green hyperelastic type. Many commonly used constitutive models for soils are based on Cauchy type of formulation. For example, different incremental isotropic nonlinear elastic stress-strain relations have been formulated based on the modification of the isotropic linear elastic relations with two of the elastic moduli (Young's modulus E, Poisson's ratio ν, shear modulus G, constrained modulus M, and bulk modulus K) being taken to be sealer functions of stress and/or strain states [5, 12, 17, 18, 19, 20].

(2) Hyperelastic (Green) type. This is based on the assumption of the existence of a strain energy density function W (or a complementary energy density function Ω) such that [4, 15]:

$$\sigma_{ij} = \frac{\partial W}{\partial \varepsilon_{ij}} \tag{2a}$$

or,

$$\varepsilon_{ij} = \frac{\partial \Omega}{\partial \sigma_{ij}} \tag{2b}$$

in which $W = \int_0^{\varepsilon_{ij}} \sigma_{ij} d\varepsilon_{ij}$ and $\Omega = \int_0^{\sigma_{ij}} \varepsilon_{ij} d\sigma_{ij}$ are functions of the current components of the strain and stress tensors, respectively. This ensures that no energy can be generated through load cycles and laws of

thermodynamics are always satisfied.

For an initially isotropic elastic material, W or Ω are expressed in terms of any three independent invariants of strain or stress tensors ε_{ij} or σ_{ij}, respectively. In general, if Ω is expressed in terms of the three stress invariants:

$$\bar{I}_1 = \sigma_{kk}$$

$$\bar{I}_2 = \frac{1}{2}\sigma_{km}\,\sigma_{km} \tag{3}$$

$$\bar{I}_3 = \frac{1}{3}\sigma_{km}\,\sigma_{kn}\,\sigma_{mn}$$

then, Eq. (2b) yields the following constitutive law

$$\varepsilon_{ij} = \frac{\partial\Omega}{\partial\bar{I}_1}\frac{\partial\bar{I}_1}{\partial\sigma_{ij}} + \frac{\partial\Omega}{\partial\bar{I}_2}\frac{\partial\bar{I}_2}{\partial\sigma_{ij}} + \frac{\partial\Omega}{\partial\bar{I}_3}\frac{\partial\bar{I}_3}{\partial\sigma_{ij}} = \phi_1\delta_{ij} + \phi_2\sigma_{ij} + \phi_3\sigma_{im}\sigma_{jm} \tag{4}$$

where the material response functions, ϕ_i, are defined as

$$\phi_i = \phi_i(\bar{I}_j) = \frac{\partial\Omega}{\partial\bar{I}_i} \tag{5}$$

and these functions are related through the three equations: [4]

$$\frac{\partial\phi_i}{\partial\bar{I}_j} = \frac{\partial\phi_j}{\partial\bar{I}_i} \tag{6}$$

In Eq. (4), δ_{ij} is the Kronecker Delta ($\delta_{11} = 1$, $\delta_{12} = 0$, etc.).

The choice of the three independent stress invariants appearing in Eqs. (3 and 4) is arbitrary. Instead, one may use the invariants $J_1 = s_{kk}$, $J_2 = \frac{1}{2}\,s_{ij}s_{ij}$ and $J_3 = \frac{1}{3}s_{ij}s_{ik}s_{jk}$ of the stress deviator tensor $s_{ij} = \sigma_{ij} - \frac{1}{3}\sigma_{kk}\delta_{ij}$, or even mixed invariants such as $\bar{I}_1$, J_2 and J_3. The particular advantage of the choice here is the separation of the functions

ϕ_i in a simple convenient manner. Based on assumed polynomial expansions of the function Ω in terms of the three invariants, different constitutive models can be developed. In particular, Evans and Pister [16] developed a general third-order stress-strain law using Eq. (4) and retaining terms in Ω from second to fourth order in stress. Ko and Masson [23] used this law and described the fitting procedure of the model and applied it to describe the behavior of Ottawa sand. This same model and fitting procedure [23] will be used in the present paper to describe the behavior of three different types of soils.

(3) Incremental (Hypoelastic) type. This type of formulation is often used to describe the mechanical behavior of a class of materials in which the state of stress depends on the current state of strain as well as on the stress path followed to reach that state [4, 6, 15, 31]. In general, the incremental constitutive relations for time-independent materials are written as [6, 12]:

$$F(\sigma_{ij}, \dot{\sigma}_{kl}, \varepsilon_{mn}, \dot{\varepsilon}_{pq}) = 0 \qquad (7)$$

provided that this equation is homogeneous in time (i.e., time occurs to the same order in all terms of the equation and therefore, may be eliminated). In Eq. (7), $\dot{\sigma}_{kl}$ and $\dot{\varepsilon}_{pq}$ are the stress increment and strain increment tensors, respectively, and F is a tensor function. Equation (7) is very general, but because of its complexity it is not possible to indicate in which manner the total and incremental stresses and strains are related and therefore, for simplicity, special cases of the general law are usually used. In particular, four special cases of the general law, in which strain increments are linearly related to stress increments through the material response moduli which depend on a single state

variable, will be given. These cases are described by the relations [6]:

$$\mathring{\sigma}_{ij} = A_{ijkl}(\sigma_{mn})\ \dot{\varepsilon}_{kl} \tag{8a}$$

$$\mathring{\sigma}_{ij} = B_{ijkl}(\varepsilon_{mn})\ \dot{\varepsilon}_{kl} \tag{8b}$$

$$\dot{\varepsilon}_{ij} = C_{ijkl}(\varepsilon_{mn})\ \mathring{\sigma}_{kl} \tag{8c}$$

$$\dot{\varepsilon}_{ij} = D_{ijkl}(\sigma_{mn})\ \mathring{\sigma}_{kl} \tag{8d}$$

where A_{ijkl} through D_{ijkl} are general functions of their indicated argument. The behavior described by any of Eqs. (8) is infinitesimally (or incrementally) reversible. This justifies the use of the suffix "elastic" in the term hypoelastic used by Truesdell [31] to describe the constitutive relations in Eq. (8a). Based on the degree of dependence of the tensorial functions A_{ijkl} through D_{ijkl} upon the components of the corrresponding tensor argument, different types of constitutive laws are obtained. For example, in a grade one (or first order) constitutive law, the tensorial functions in Eqs. (8) are linear functions of their arguments. A hypoelastic material of grade zero (zero order) is equivalent to anisotropic elastic Cauchy material. Hook's Law is representative of this type of behavior in case of isotropic materials. For isotropic materials, the tensorial response functions in Eqs. (8) are further restricted to be form-invariant under the full group of transformation of the coordinate axes [4].

Several incremental constitutive relations have been used in modelling the behavior of soils and rocks [1, 6, 7, 19, 28, 32]. More recently, incremental stress-strain relations have been formulated separately for a special class of the hypoelastic materials, in which the response tensors in Eqs. (8) are assumed to depend on the invariants, but

not on the stress (or strain) tensor itself. However, in these later models, different forms for the material response functions apply in initial loading, and in subsequent unloading and reloading, i.e., the models are generally irreversible, even for incremental loading. These models are now known as variable-moduli models, and they have been extensively used to describe the behavior of soils in ground shock studies [26, 27]. In Ref. [4], a complete critical theoretical study of the three types of elasticity formulation has been made.

In the first part of the following discussions, a third-order hyperelastic (Green) constitutive model is formulated (sec. 2), and specific fitting procedure to determine the material constants together with several numerical examples are subsequently described (sec. 3). Based on this formulation, explicit expression is developed for the incremental stress-strain relation (sec. 4). This model is subsequently refined by introducing a loading criterion and a failure criterion, thus, extending the range of application to reversed loading case (sec. 5). In the second part, theoretical considerations of the model for uniqueness and stability of numerical solutions are examined (sec. 6). Comparisons of the model predictions with experimental results are made in sec. 7. Advantages and limitations of the deformational types of plasticity models, which are identical with nonlinear elastic types of stress-strain relations as long as unloading does not occur, are emphasized. The model described in this paper can be readily applied to nonlinear stress analysis of geotechnical problems involving three-dimensional stress and strain components.

2. Formulation of the Proposed Third-Order Hyperelastic (Green) Constitutive Model

2.1 General

For an initially isotropic material, if the complementary energy function $\Omega(\bar{I}_1, \bar{I}_2, \bar{I}_3)$ is expressed as a fourth order polynominal in the stress components, one can write [16, 23]:

$$\Omega(\bar{I}_1, \bar{I}_2, \bar{I}_3) = A_0 + A_1\bar{I}_1 + \tfrac{1}{2}B_1\bar{I}_1^2 + \tfrac{1}{3}B_2\bar{I}_1^3 + B_3\bar{I}_1\bar{I}_2 + B_4\bar{I}_2 + B_5\bar{I}_3 + \tfrac{1}{4}B_6\bar{I}_1^4 + B_7\bar{I}_1^2\bar{I}_2 + \tfrac{1}{2}B_8\bar{I}_2^2 + B_9\bar{I}_1\bar{I}_3 \tag{9}$$

where the stress invariants $\bar{I}_1$, $\bar{I}_2$ and $\bar{I}_3$ are defined in Eqs. (3) and A_0, A_1 and B_1 to B_9 are material constants. The numerical values of the coefficients in Eq. (9) above are inserted for convenience in subsequent derivation. Then, using the normality condition of Eq. (2b), the constitutive relations may be written as:

$$\varepsilon_{ij} = A_1\delta_{ij} + [B_1\bar{I}_1 + B_2\bar{I}_1^2 + B_3\bar{I}_2 + B_6\bar{I}_1^3 + 2B_7\bar{I}_1\bar{I}_2 + B_9\bar{I}_3]\delta_{ij} + [B_3\bar{I}_1 + B_4 + B_7\bar{I}_1^2 + B_8\bar{I}_2]\sigma_{ij} + [B_5 + B_9\bar{I}_1]\sigma_{im}\sigma_{jm} \tag{10}$$

Assuming that the initial stress-free state corresponds to initial strain-free state, the constant A_1 is equal to zero, and we have from Eq. (10),

$$\varepsilon_{ij} = \phi_1\sigma_{ij} + \phi_2\sigma_{ij} + \phi_3\sigma_{im}\sigma_{jm} \tag{11a}$$

where the material response functions, ϕ_i, of Eq. (4), are given by

$$\phi_1 = B_1\bar{I}_1 + B_2\bar{I}_1^2 + B_3\bar{I}_2 + B_6\bar{I}_1^3 + 2B_7\bar{I}_1\bar{I}_2 + B_9\bar{I}_3 \tag{11b}$$

$$\phi_2 = B_3\bar{I}_1 + B_4 + B_7\bar{I}_1^2 + B_8\bar{I}_2 \tag{11c}$$

$$\phi_3 = B_5 + B_9\bar{I}_1 \tag{11d}$$

and obviously the relations between these functions, Eqs. (6), are satisfied. Equations (11a to d) are the general third-order hyperelastic (Green) stress-strain relations. It only remains to determine the nine material constants B_1 to B_9 from experimental results in order to complete the model formulation. This will be explained in subsequent sections. The general form of the proposed third-order constitutive law, Eqs. (11), was formulated by Evans and Pister [16]. The present formulation of the model and the procedure of determining the nine material constants B_1 to B_9 follow the method originally developed by Ko and Masson [23].

As mentioned in [23], based on the experimental test results, stress-strain curves describing the behavior of many soils especially loose sands and soft clays in shearing along conventional soil tests (e.g., triaxial compression, triaxial extension, and simple shear tests) can be best represented by odd functions. For instance, typical stress-strain curves for soil along different shearing stress path (Fig. 1a, b) are illustrated in Fig. 1(c) for Ottawa sand [23]. This is the reason for the particular choice of the third-order stress-strain law.

For most soils (and particularly for cohesionless soils) initial natural state includes a nonzero reference state of stress, σ^0_{ij}, corresponding to a zero reference state of strain $\varepsilon_{ij}(\sigma^0_{kl})$. Therefore, the components of the incremental strains $\Delta\varepsilon_{ij}$ corresponding to the incremental stresses $\Delta\sigma_{ij}$ measured from the initial reference state of stress, σ^0_{ij}, are calculated as:

$$\Delta\varepsilon_{ij}(\sigma^0_{kl}, \Delta\sigma_{kl}) = \varepsilon_{ij}(\sigma^0_{kl} + \Delta\sigma_{kl}) - \varepsilon_{ij}(\sigma^0_{kl}) \qquad (12)$$

Substituting σ^0_{kl} and $\Delta\sigma^0_{kl}$ into Eq. (11a) to calculate the corresponding

strains $\varepsilon_{ij}(\sigma^0_{kl})$ and $\varepsilon_{ij}(\sigma^0_{kl} + \Delta\sigma_{kl})$, Eq. (12) can be written in the form:

$$\Delta\varepsilon_{ij}(\sigma^0_{kl} + \Delta\sigma_{kl}) = (\tilde{\phi}_1 - \phi_1)\delta_{ij} + (\tilde{\phi}_2 - \phi_2)\sigma^0_{ij} + \tilde{\phi}_2\Delta\sigma_{ij} + (\tilde{\phi}_3 - \phi_3)\sigma^0_{im}\sigma^0_{jm} + \tilde{\phi}_3(\sigma^0_{im}\Delta\sigma_{jm} + \sigma^0_{jm}\Delta\sigma_{im} + \Delta\sigma_{im}\Delta\sigma_{jm}) \tag{13a}$$

where,

$$\tilde{\phi}_1 = \phi_1(\sigma^0_{kl} + \Delta\sigma_{kl}) \;;\; \tilde{\phi}_2 = \phi_2(\sigma^0_{kl} + \Delta\sigma) \;;\; \tilde{\phi}_3 = \phi_3(\sigma^0_{kl} + \Delta\sigma_{kl})$$
$$\phi_1 = \phi_1(\sigma^0_{kl}) \;;\; \phi_2 = \phi_2(\sigma^0_{kl}) \;;\; \phi_3 = \phi_3(\sigma^0_{kl}) \tag{13b}$$

i.e., the functions $\tilde{\phi}_i$ and ϕ_i are computed by substituting the corresponding states of stress, $(\sigma^0_{kl} + \Delta\sigma)$ and σ^0_{kl}, respectively, into the expressions of Eqs. (11b to d). It is to be emphasized that $\Delta\varepsilon_{ij}(\sigma^0_{kl} + \Delta\sigma)$ are not incremental strains in a complete sense; they represent total strains measured from the initial reference state, σ^0_{kl}, with the components $\varepsilon_{ij}(\sigma^0_{kl})$ taken as zero. The stress components $\Delta\sigma_{ij}$ are not necessarily small.

In order to study the behavior of the stress-strain model of Eq. (13) under the conditions of conventional soil tests, it is necessary to reduce the relations for the particular loading paths followed in these tests. Since the stress paths in most soil tests are straight line paths in the principal stress space (e.g., CTC, CTE, SS, HC, etc.), it is more convenient to develop the stress-strain relations of the model under a general straight line loading path in the principal stress space. Then, for a particular loading path in any test, the relations can be formulated very easily as a special case from the general straight line loading path. In the forthcoming, formulation of the constitutive relations of the model

under a general straight line (proportional) loading path is given. In addition, examples of specific relations in a number of conventional tests are presented.

2.2 Stress-Strain Relation for a General Straight Line Loading Path in the Principal Stress Space

In the formulation presented here, the initial reference state of stress, σ^0_{kl}, is assumed to be a hydrostatic stress state (since all the tests performed satisfy this condition); i.e.,

$$\sigma^0_{ij} = \sigma_c \quad (\text{or } \sigma^0_1 = \sigma^0_2 = \sigma^0_3 = \sigma_c);\ \text{for } i = j$$
$$\sigma^0_{ij} = 0;\ \text{for } i \neq j \tag{13}$$

where σ_1, σ_2 and σ_3 are the principal major, intermediate and minor stresses, respectively, and σ_c denotes the initial consolidation pressure.

Denote the increment stress $\Delta\sigma_1$ in the major principal stress measured from the initial hydrostatic state of stress by λ. Then, for a general straight line stress path, the increments $\Delta\sigma_1$ and $\Delta\sigma_2$ in the other two principal stress are $\alpha_1\lambda$ and $\alpha_2\lambda$, respectively; i.e.,

$$\Delta\sigma_1 : \Delta\sigma_2 : \Delta\sigma_3 = 1 : \alpha_1 : \alpha_2 \tag{14}$$

where α_1 and α_2 are parameters determining the direction of the straight line path (Fig. 2). Thus, the invariants $\bar{I}_1$, $\bar{I}_2$ and $\bar{I}_3$ of Eqs. (3) for the intial and current states of stress σ^0_{kl} and $\sigma_{kl} + \Delta\sigma^0_{kl}$, respectively, as shown in Fig. 2, are given by

$$\bar{I}_1(\sigma^0_{kl}) = 3\sigma_c\ ,\quad \bar{I}_2(\sigma^0_{kl}) = \frac{3}{2}\sigma_c^2\ ,\quad \bar{I}_3(\sigma^0_{kl}) = \sigma_c^3$$

$$\bar{I}_1(\sigma^0_{kl} + \Delta\sigma_{kl}) = 3\sigma_c + 3\lambda k_1$$

$$\bar{I}_2(\sigma^0_{kl} + \Delta\sigma_{kl}) = \frac{3}{2}\sigma_c^2 + \sigma_c\lambda k_1 + \frac{1}{2}\lambda^2 k_2 \qquad (15a)$$

$$\bar{I}_3(\sigma^0_{kl} + \Delta\sigma_{kl}) = \sigma_c^3 + \sigma_c^2\lambda k_1 + \sigma_c\lambda^2 k_2 + \frac{1}{3}\lambda^3 k_3$$

in which the parameters k_1, k_2 and k_3 are defined as

$$k_1 = 1 + \alpha_1 + \alpha_2$$

$$k_2 = 1 + \alpha_1^2 + \alpha_2^2 \qquad (15b)$$

$$k_3 = 1 + \alpha_1^3 + \alpha_2^3$$

Hence, substituting the expressions (15a, b) into Eqs. (13b) and using Eq. (13a) to calculate the principal strains $\Delta\varepsilon_1$, $\Delta\varepsilon_2$ and $\Delta\varepsilon_3$, we finally get

$$\Delta\varepsilon_1 = C_1^{(1)}\lambda + C_2^{(1)}\lambda^2 + C_3^{(1)}\lambda^3$$

$$\Delta\varepsilon_2 = C_1^{(2)}\lambda + C_2^{(2)}\lambda^2 + C_3^{(2)}\lambda^3 \qquad (16a)$$

$$\Delta\varepsilon_3 = C_1^{(3)}\lambda + C_2^{(3)}\lambda^2 + C_3^{(3)}\lambda^3$$

in which the $C_j^{(i)}$ coefficients are given by

$$C_1^{(1)} = (k_1B_1 + B_4) + [6k_1B_2 + (2k_1 + 3)B_3 + 2B_5]\sigma_c + [27k_1B_6 + (15k_1 + 9)B_7 + (k_1 + \tfrac{3}{2})B_8 + (2k_1 + 6)B_9]\sigma_c^2$$

$$C_2^{(1)} = [k_1^2B_2 + (k_1 + \tfrac{1}{2}k_2)B_3 + B_5] + [9k_1^2B_6 + (6k_1 + 3k_1^2 + 3k_2)B_7 + (k_1 + \tfrac{1}{2}k_2)B_8 + (2k_1 + k_2 + 3)B_9]\sigma_c$$

$$C_3^{(1)} = k_1^3 B_6 + (k_1^2 + k_1 k_2) B_7 + \tfrac{1}{2} k_2 B_8 + (k_1 + \tfrac{1}{3} k_3) B_9$$

$$C_1^{(2)} = (k_1 B_1 + \alpha_1 B_4) + [6k_1 B_2 + (2k_1 + 3\alpha_1) B_3 + 2\alpha_1 B_5]\sigma_c$$

$$+ [27k_1 B_6 + (15k_1 + 9\alpha_1) B_7 + (k_1 + \tfrac{3}{2}\alpha_1) B_8 + (2k_1 + 6\alpha_1) B_9]\sigma_c^2$$

$$C_2^{(2)} = [k_1^2 B_2 + (\alpha_1 k_1 + \tfrac{1}{2} k_2) B_3 + \alpha_1^2 B_5] + [9k_1^2 B_6 + (6\alpha_1 k_1 + 3k_1^2 + 3k_2) B_7$$

$$+ (\alpha_1 k_1 + \tfrac{1}{2} k_2) B_8 + (3\alpha_1^2 + 2\alpha_1 k_1 + k_2) B_9]\sigma_c$$

$$C_3^{(2)} = k_1^3 B_6 + (k_1 k_2 + \alpha_1 k_1^2) B_7 + \tfrac{1}{2}\alpha_1 k_2 B_8 + (\alpha_1^2 k_1 + \tfrac{1}{3} k_3) B_9 \qquad (16b)$$

$$C_1^{(3)} = (k_1 B_1 + \alpha_2 B_4) + [6k_1 B_2 + (2k_1 + 3\alpha_2) B_3 + 2\alpha_2 B_5]\sigma_c$$

$$+ [27k_1 B_6 + (15k_1 + 9\alpha_2) B_7 + (k_1 + \tfrac{3}{2}\alpha_2) B_8 + (2k_1 + 6\alpha_2) B_9]\sigma_c^2$$

$$C_2^{(3)} = [k_1^2 B_2 + (\alpha_2 k_1 + \tfrac{1}{2} k_2) B_3 + \alpha_2^2 B_5] + [9k_1^2 B_6 + (6\alpha_2 k_1 + 3k_1^2 + 3k_2) B_7$$

$$+ (\alpha_2 k_1 + \tfrac{1}{2} k_2) B_8 + (3\alpha_2^2 + 2\alpha_2 k_1 + k_2) B_9]\sigma_c$$

$$C_3^{(3)} = k_1^3 B_6 + (k_1 k_2 + \alpha_2 k_1^2) B_7 + \tfrac{1}{2}\alpha_2 k_2 B_8 + (\alpha_2^2 k_1 + \tfrac{1}{3} k_3) B_9$$

Clearly, the advantage of performing the tests along straight line loading paths is that the changes in the principal stress and strain components during the tests are conveniently expressed in terms of a single parameter, λ, as given in Eqs. (14) and (16a). Furthermore, the components of the principal strain increments are given as cubic functions in this parameter (see Eq. 16a). Indeed, these cubic relations are the basis for the determination of the nine material constants, B_i, from the experimental results, as will be explained later.

In the following, special cases of the relations of Eq. (16) are given for some of the stress paths in the conventional soil tests.

(a) Hydrostatic Compression Path (HC): Fig 1(a)

In this case, the stress components $\sigma_1 = \sigma_2 = \sigma_3$ are increasing and $\alpha_1 = \alpha_2 = 1$, $k_1 = k_2 = k_3 = 3$. Thus, Eqs. (16) simplify to

$$\begin{aligned}\Delta\varepsilon_1 = \Delta\varepsilon_2 = \Delta\varepsilon_3 = {} & [(3B_1 + B_4) + (18B_2 + 9B_3 + 2B_5)\sigma_c \\ & + (81B_6 + 54B_7 + \tfrac{9}{2}B_8 + 12B_9)\sigma_c^2]\lambda + [(9B_2 + \tfrac{9}{2}B_3 + B_5) \\ & + (81B_6 + 54B_7 + \tfrac{9}{2}B_8 + 12B_9)\sigma_c]\lambda^2 \\ & + [27B_6 + 18B_7 + \tfrac{3}{2}B_8 + 4B_9]\lambda^3\end{aligned} \tag{17}$$

(b) Conventional Triaxial Compression Path (CTC): Fig. 1(a)

The components $\sigma_2 = \sigma_3$ are constant, and σ_1 is increasing; i.e., $\alpha_1 = \alpha_2 = 0$, $k_1 = k_2 = k_3 = 1$. Hence, for $\sigma_1^0 = \sigma_2^0 = \sigma_3^0 = \sigma_c$ and $\Delta\sigma_1 = \lambda$, we have from Eqs. (16)

$$\begin{aligned}\Delta\varepsilon_1 = {} & [(B_1 + B_4) + (6B_2 + 5B_3 + 2B_5)\sigma_c + (27B_6 + 24B_7 + \tfrac{5}{2}B_8 + 8B_9)\sigma_c^2]\lambda \\ & + [(B_2 + \tfrac{3}{2}B_3 + B_5) + (9B_6 + 12B_7 + \tfrac{3}{2}B_8 + 6B_9)\sigma_c]\lambda^2 \\ & + [B_6 + 2B_7 + \tfrac{1}{2}B_8 + \tfrac{4}{3}B_9]\lambda^3 \\ \Delta\varepsilon_2 = \Delta\varepsilon_3 = {} & [B_1 + (6B_2 + 2B_3)\sigma_c + (27B_6 + 15B_7 + B_8 + 2B_9)\sigma_c^2]\lambda \\ & + [(B_2 + \tfrac{1}{2}B_3) + (9B_6 + 6B_7 + \tfrac{1}{2}B_8 + B_9)\sigma_c]\lambda^2 \\ & + [B_6 + B_7 + \tfrac{1}{3}B_9]\lambda^3\end{aligned} \tag{18}$$

(c) Simple Shear Path (SS): Fig. 1(b)

The stress component σ_1 is increasing, and σ_3 is decreasing while σ_2 is held constant; i.e., $\alpha_1 = 0$, $\alpha_2 = -1$. Therefore, the equations in (16) are reduced to: ($k_1 = k_3 = 0$, $k_2 = 2$)

$$\Delta\varepsilon_1 = [B_4 + (3B_3 + 2B_5)\sigma_c + (9B_7 + \tfrac{3}{2}B_8 + 6B_9)\sigma_c^2]\lambda$$
$$+ [(B_3 + B_5) + (6B_7 + B_8 + 5B_9)\sigma_c]\lambda^2 + [B_8]\lambda^3$$
$$\Delta\varepsilon_2 = [B_3 + (6B_7 + B_8 + 2B_9)\sigma_c]\lambda^2 \qquad (19)$$
$$\Delta\varepsilon_3 = -[B_4 + (3B_3 + 2B_5)\sigma_c + (9B_7 + \tfrac{3}{2}B_8 + 6B_9)\sigma_c^2]\lambda$$
$$+ [(B_3 + B_5) + (6B_7 + B_8 + 5B_9)\sigma_c]\lambda^2 - [B_8]\lambda^3$$

(d) Triaxial Compression Path With Constant Mean Normal Stress (TC):

Fig. 1(a, b)

In this case, the component σ_1 is increasing while $\sigma_2 = \sigma_3$ are decreasing such that $\sigma_1 + \sigma_2 + \sigma_3 = \text{const.} = 3\sigma_c$; i.e., $\Delta\sigma_1 + \Delta\sigma_2 + \Delta\sigma_3 = 0$; or $\alpha_1 = \alpha_2 = -\frac{1}{2}$ and $k_1 = 0$, $k_2 = \frac{3}{2}$, $k_3 = \frac{3}{4}$. Then, we have

$$\Delta\varepsilon_1 = [B_4 + (3B_3 + 2B_5)\sigma_c + (9B_7 + \tfrac{3}{2}B_8 + 6B_9)\sigma_c^2]\lambda$$
$$+ [(\tfrac{3}{4}B_3 + B_5) + (\tfrac{9}{2}B_7 + \tfrac{3}{4}B_8 + \tfrac{9}{2}B_9)\sigma_c]\lambda^2 + [\tfrac{3}{4}B_8 + \tfrac{1}{4}B_9]\lambda^3$$
$$\Delta\varepsilon_2 = \Delta\varepsilon_3 = -[\tfrac{1}{2}B_4 + (\tfrac{3}{2}B_3 + B_5)\sigma_c + (\tfrac{9}{2}B_7 + \tfrac{3}{4}B_8 + 3B_9)\sigma_c^2]\lambda \qquad (20)$$
$$+ [(\tfrac{3}{4}B_3 + \tfrac{1}{4}B_5) + (\tfrac{9}{2}B_7 + \tfrac{3}{4}B_8 + \tfrac{9}{4}B_9)\sigma_c]\lambda^2$$
$$+ [-\tfrac{3}{8}B_8 + \tfrac{1}{4}B_9]\lambda^3$$

(e) Triaxial Extension Path With Constant Mean Normal Stress (TE):

Fig. 1(a, b)

The component σ_1 is decreasing while $\sigma_2 = \sigma_3$ are increasing such that $\sigma_1 + \sigma_2 + \sigma_3 = \text{const.} = 3\sigma_c$. Denoting the change (decrease) in σ_1 by λ (i.e., $\Delta\sigma_1 = -\lambda$), then $\alpha_1 = \alpha_2 = -\frac{1}{2}$ and $k_1 = 0$, $k_2 = \frac{3}{2}$, $k_3 = \frac{3}{4}$ and the strain increments are:

$$\Delta\varepsilon_1 = -[B_4 + (3B_3 + 2B_5)\sigma_c + (9B_7 + \tfrac{3}{2}B_8 + 6B_9)\sigma_c^2]\lambda$$
$$+ [(\tfrac{3}{4}B_3 + B_5) + (\tfrac{9}{2}B_7 + \tfrac{3}{4}B_8 + \tfrac{9}{2}B_9)\sigma_c]\lambda^2 - [\tfrac{3}{4}B_8 + \tfrac{1}{4}B_9]\lambda^3$$
$$\Delta\varepsilon_2 = \Delta\varepsilon_3 = [\tfrac{1}{2}B_4 + (\tfrac{3}{2}B_3 + B_5)\sigma_c + (\tfrac{9}{2}B_7 + \tfrac{3}{4}B_8 + 3B_9)\sigma_c^2]\lambda \qquad (21)$$
$$+ [(\tfrac{3}{4}B_3 + \tfrac{1}{4}B_5) + (\tfrac{9}{2}B_7 + \tfrac{3}{4}B_8 + \tfrac{9}{4}B_9)\sigma_c]\lambda^2 + [\tfrac{3}{8}B_8 - \tfrac{1}{4}B_9]\lambda^3$$

3. Fitting Procedure to Determine Material Constants

3.1 Fitting Procedure

The procedure of the determination of the nine material constants, B_i, is outlined in Ref. [23]. In this section, this procedure is summarized and the results obtained for the three different soils: clay "X", clay "Y" and Ottawa sand are given.

(a) Along a straight line stress path in any test, the principal strain increments $\Delta\varepsilon_1$, $\Delta\varepsilon_2$ and $\Delta\varepsilon_3$ are expressed as cubic functions of the parameter λ, as given in Eq. (16a), with the appropriate constants C_1, C_2 and C_3 according to the particular type of the test. Moreover, the constants C_i, which depend on the reference inital state of stress in the test, σ_{ij}^0, and the orientation of the loading path (defined by α_1 and α_2), are then linearly related to the nine material constants, B_i, using Eqs. (16b).

(b) By fitting cubic curves to the experimentally obtained stress-strain curves for each component of the principal strain increments, the numerical values of the three distinct constants C_1, C_2 and C_3 for this component are determined. Standard procedures of regression analysis may be used in fitting the cubic curves. However, it was found that the initial slopes of the curves determined from such analyses usually deviate too much from the measured slopes. Therefore, the procedure employed here is

based on matching the initial slope and two points for each curve to determine the three constants C_1, C_2 and C_3, as shown in Fig. 3. In some cases, adjustment of the determined constants may be made to give a better overall fit to the experimental curves.

(c) From the results obtained in (a) and (b) above, we have a number of linear simultaneous equations in the nine unknowns, B_i (three equations for each distinct stress-strain curve). Theoretically, since nine unknown independent material constants are present, only three independent stress-strain curves are required to give nine equations in nine independent unknowns. These three curves are completely arbitrary and they could be from any type of test. However, it is not expected that a constitutive model with its constants determined from one test is capable of predicting the behavior of the material under arbitrary loading paths different from that of the test. Thus, it is better to make use of most of the available test results, in which case the number of linear equations will exceed the number of unknown independent material constants.

(d) The system of linear equations obtained in (c) (which generally exceeds the number of unknown material constants, B_i) is solved using a least-square solution technique to determine the nine material constants B_i.

3.2 Numerical Results

The procedure described above has been applied to the three types of soils mentioned earlier. The test conditions and the numerical results obtained for each are summarized in the forthcoming.

(a) Clay "X"

The experimental data for this soil were obtained from triaxial tests with constant mean normal stress under consolidated drained conditions

conducted on prismatic samples trimmed from block samples. The samples were 100% saturated. During the tests, the measured quantities were the principal stress components σ_1, σ_2 and σ_3 (the major principal stress σ_1 is in the vertical direction while σ_2 and σ_3 are in the lateral directions), the principal strains ε_1 and ε_3, and the volumetric strains $\varepsilon_v = \varepsilon_{kk}$ (the signs follow the soil mechanics sign convention, i.e., compressive stresses and strains are positive).

The tests were performed under constant stress ratio, m, where m is defined as

$$m = \frac{\sigma_2 - \sigma_3}{\sigma_1 - \sigma_3} \tag{22}$$

six different sets of data are provided for clay "X": two sets with m = 0, 1 for each one of the initial hydrostatic (consolidation) stress σ_c = 10, 20, 30 psi. Note that for drained conditions total stresses, σ_{ij}, and effective stresses, σ'_{ij}, are equal. The effective stresses, σ'_{ij}, are given by

$$\sigma'_{ij} = \sigma_{ij} - u\delta_{ij} \tag{23}$$

where u is the pore water pressure.

As can be noted from Eqs. (20), for the TC tests, only six material constants, B_3, B_4, B_5, B_7, B_8 and B_9 are used. Thus, the least-square solution procedure is used for 36 equations in 6 unknowns (six equations for each set of data after allowing for symmetry in the tests). The results obtained are:

$$B_3 = 4.4073 \times 10^{-5} \text{ psi}^{-2} , \quad B_4 = 8.5 \times 10^{-5} \text{ psi}^{-1} ,$$

$$B_5 = -5.861 \times 10^{-5} \text{ psi}^{-2} , \quad B_7 = -4.3667 \times 10^{-6} \text{ psi}^{-3} ,$$

$$B_8 = 2.8092 \times 10^{-5} \text{ psi}^{-3} \quad , \quad B_9 = 3.478 \times 10^{-7} \text{ psi}^{-3}$$

These values of material constants are used in the prediction of stress-strain curves for m = 0.25, 0.50, 0.75 for each value of σ_c = 10, 20, 30 psi, as shown in Fig. 4(a).

(b) Clay "Y"

As for clay "X", 100% saturated prismatic samples were tested under consolidated drained conditions. The tests were of the conventional tri-axial type in which the minor principal stress, σ_3, was kept constant.

Six different sets of data were available for clay "Y": two sets with m = 0, 1 for σ_c = 2.5, 5, 10 psi. The results obtained for the solution of 36 equations in 9 unknown material constants are:

$$B_1 = - 3.7425 \times 10^{-4} \text{ psi}^{-1} \quad , \quad B_2 = - 6.69 \times 10^{-7} \text{ psi}^{-2} \quad ,$$

$$B_3 = 5.5416 \times 10^{-5} \text{ psi}^{-2} \quad , \quad B_4 = 6.913 \times 10^{-4} \text{ psi}^{-1} \quad ,$$

$$B_5 = -1.3109 \times 10^{-4} \text{ psi}^{-2} \quad , \quad B_6 = 1.164 \times 10^{-6} \text{ psi}^{-3}$$

$$B_7 = -3.954 \times 10^{-6} \text{ psi}^{-3} \quad , \quad B_8 = 1.254 \times 10^{-5} \text{ psi}^{-3} \quad ,$$

$$B_9 = 3.9257 \times 10^{-6} \text{ psi}^{-3}$$

These values are used to predict the material behavior for m = 0.25, 0.5, 0.75 under the initial consolidation stresses σ_c = 2.5, 5, 10 psi, as shown in Fig. 4(b).

(c) Ottawa Sand

Samples of Ottawa sand were compacted by aerial pluviation to a relative density of 87% and they were tested in the dry state three-dimensionally under different stress paths. The data sets provided were

for different stress paths: CTC, CTE, HC, TC and TE, for varieties of initial hydrostatic stresses, σ_c. For example, the CTC tests were carried out for σ_c = 5 and 10 psi, and σ_c = 10 psi was used for the CTE test. Both the TC and TE tests were performed for 3 values of the initial equal hydrostatic pressure, σ_c = 5, 10, 20 psi. The principal axes are denoted by z (vertical) and x, y (horizontal).

For Ottawa sand, the material constants reported in Ref. [20] were tried and reasonably good overall agreement of the theoretical curves and the experimental results provided was obtained. Therefore, it was decided to use these same values instead of the values initially obtained from separate least square solutions of the equations. This provides means for further investigation of the range of applicability of the model. For instance, although these values of the constants yielded reasonably good results for most of the cases discussed in [23] and for those of the test cases for model calibration investigated here, it was found that the behavior of the model is sensitive to the small changes of the constants of the higher order terms (e.g., B_6, B_7, B_8 and B_9). Slight changes in the values of these constants will change greatly the behavior of the model under certain stress paths. This will be illustrated in the second part of the present paper. The values of the constants reported in [23] are:

$$B_1 = -4.431 \times 10^{-5}\ \text{psi}^{-1},\ B_2 = 1.685 \times 10^{-6}\ \text{psi}^{-2},\ B_3 = -3.107 \times 10^{-6}\ \text{psi}^{-2}$$

$$B_4 = 1.885 \times 10^{-4}\ \text{psi}^{-1},\ B_5 = 1.725 \times 10^{-6}\ \text{psi}^{-2},\ B_6 = 0.1237 \times 10^{-6}\ \text{psi}^{-3}$$

$$B_7 = -0.4018 \times 10^{-6}\ \text{psi}^{-3},\ B_8 = 2.578 \times 10^{-7}\ \text{psi}^{-3},\ B_9 = 5.597 \times 10^{-9}\ \text{psi}^{-3}$$

For the study of the effect of the change in the numerical values of the material constants on the results, the values of the constants B_6 and B_7

were changed to $B_6 = 0.1687 \times 10^{-6}$ and $B_7 = -0.4690 \times 10^{-6}$ without changing the other constants. The stress paths used in the prediction are shown in Fig. 4(c).

4. Incremental Form of the Stress-Strain Relations

The ultimate goal of developing constitutive models is its use in the solution of a boundary value problem to predict the behavior of the structure. Most often, numerical techniques such as the finite element method are used in the solution, and incremental stress-strain relations are needed to solve problems involving material and/or geometrical non-linearities. In the following, an incremental form of the nonlinear general constitutive law of Eqs. (11) is formulated. In addition, the material compliance matrix relating the increments of the principal stresses and strains is developed.

Differentiating Eq. (11a), the strain increment tensor $\dot{\varepsilon}_{ij}$ can be written as:

$$\dot{\varepsilon}_{ij} = [\frac{\partial \phi_1}{\partial \sigma_{kl}} \delta_{ij} + \phi_2 \frac{\partial \sigma_{ij}}{\partial \sigma_{kl}} + \sigma_{ij} \frac{\partial \phi_2}{\partial \sigma_{kl}} + \phi_3 \frac{\partial (\sigma_{im} \sigma_{jm})}{\partial \sigma_{kl}} + \sigma_{im}\sigma_{jm} \frac{\partial \phi_3}{\partial \sigma_{kl}}]\dot{\sigma}_{kl} \qquad (24)$$

where $\dot{\sigma}_{kl}$ is the stress increment tensor, and the functions ϕ_i are given in Eqs. (11b to d). The partial derivatives in the equation above are calculated using the expressions for ϕ_i, and the results are given by

$$\frac{\partial \phi_1}{\partial \sigma_{kl}} = (B_1 + 2B_2\bar{I}_1 + 3B_6\bar{I}_1^2 + 2B_7\bar{I}_2)\delta_{kl} + (B_3 + 2B_7\bar{I}_1)\sigma_{kl} + B_9\sigma_{kn}\sigma_{ln}$$

$$\frac{\partial \phi_2}{\partial \sigma_{kl}} = (B_3 + 2B_7\bar{I}_1)\delta_{kl} + B_8\sigma_{kl} \qquad (25)$$

$$\frac{\partial \phi_3}{\partial \sigma_{kl}} = B_9\delta_{kl} \; ; \; \frac{\partial \sigma_{ij}}{\partial \sigma_{kl}} = \delta_{ik}\,\delta_{jl} \; ; \; \frac{\partial \sigma_{im}\sigma_{jm}}{\partial \sigma_{kl}} = \sigma_{il}\delta_{jk} + \sigma_{jl}\delta_{ik}$$

Combining the results of Eq. (24) into Eq. (25), we finally obtain

$$\dot{\varepsilon}_{ij} = [\frac{\partial \phi_1}{\partial \sigma_{kl}} \delta_{ij} + \phi_2 \delta_{ik}\delta_{jl} + \sigma_{ij} \frac{\partial \phi_2}{\partial \sigma_{kl}} + \sigma_3(\sigma_{il}\delta_{jk} + \sigma_{jl}\delta_{ik}) + \sigma_{im}\sigma_{jm} \frac{\partial \phi_3}{\partial \sigma_{kl}}]\dot{\sigma}_{kl} \tag{26}$$

This equation represents the general incremental form of the proposed nonlinear third-order hyperelastic constitutive model. This equation can always be written in a matrix form

$$\{\dot{\varepsilon}\} = [C]\{\dot{\sigma}\} \tag{27}$$

where $\{\dot{\varepsilon}\}$ and $\{\dot{\sigma}\}$ are the strain and stress increment vectors, respectively, and [C] is the material tangential compliance symmetric matrix which depends on the current state of stress σ_{ij} and the material constants B_i. Special cases such as plane stress, plane strain and axisymmetric, can be readily developed from the general form of Eq. (27). As an example, the matrix equation relating the principal stress and strain increments is written as

$$\begin{Bmatrix} \dot{\varepsilon}_1 \\ \dot{\varepsilon}_2 \\ \dot{\varepsilon}_2 \end{Bmatrix} = \begin{bmatrix} C_{11} & C_{12} & C_{13} \\ C_{21} & C_{22} & C_{23} \\ C_{31} & C_{32} & C_{33} \end{bmatrix} \begin{Bmatrix} \dot{\sigma}_1 \\ \dot{\sigma}_2 \\ \dot{\sigma}_3 \end{Bmatrix} \tag{28}$$

where the elements of symmetrix matrix [C] are given by

$$C_{11} = [(B_1 + B_4) + (2B_2 + B_3)\bar{I}_1 + (3B_6 + B_7)\bar{I}_1^2 + (2B_7 + B_8)\bar{I}_2] + [2(B_3 + B_5) + 2(2B_7 + B_9)\bar{I}_1]\sigma_1 + (B_8 + 2B_9)\sigma_1^2$$

$$C_{22} = [B_1 + B_4) + (2B_2 + B_3)\bar{I}_1 + (3B_6 + B_7)\bar{I}_1^2 + (2B_7 + B_8)\bar{I}_2]$$
$$+ [2(B_3 + B_5) + 2(2B_7 + B_9)\bar{I}_1]\sigma_2 + (B_8 + 2B_9)\sigma_2^2$$

$$C_{33} = [(B_1 + B_4) + (2B_2 + B_3)\bar{I}_1 + (3B_6 + B_7)\bar{I}_1^2 + (2B_7 + B_8)\bar{I}_2]$$
$$+ [2(B_3 + B_5) + 2(2B_7 + B_9)\bar{I}_1]\sigma_3 + (B_8 + 2B_9)\sigma_3^2 \qquad (28a)$$

$$C_{12} = C_{21} = [B_1 + 2B_2\bar{I}_1 + 3B_6\bar{I}_1^2 + 2B_7\bar{I}_2] + (B_3 + 2B_7\bar{I}_1)(\sigma_1 + \sigma_2)$$
$$+ B_8\sigma_1\sigma_2 + B_9(\sigma_1^2 + \sigma_2^2)$$

$$C_{13} = C_{31} = [B_1 + 2B_2\bar{I}_1 + 3B_6\bar{I}_1^2 + 2B_7\bar{I}_2] + (B_3 + 2B_7\bar{I}_1)\ (\sigma_1 + \sigma_3)$$
$$+ B_8\sigma_1\sigma_3 + B_9(\sigma_1^2 + \sigma_3^2)$$

$$C_{23} = C_{32} = [B_1 + 2B_2\bar{I}_1 + 3B_6\bar{I}_1^2 + 2B_7\bar{I}_2] + (B_3 + 2B_7\bar{I}_1)(\sigma_2 + \sigma_3)$$
$$+ B_8\sigma_2\sigma_3 + B_9(\sigma_2^2 + \sigma_3^2).$$

It is to be emphasized that the previous equations are valid only for the case when the principal axes of stresses and strains coincide and do not rotate as the material element deforms. In such cases, the principal axes of strain and stress increments also coincide. In general, the principal axes of stress and strain increments do not coincide; shearing stress increments will produce volumetric strains in addition to the shearing strains, and deviatoric and hydrostatic components of the response are always coupled. Such interaction and cross effects between the deviatoric and hydrostatic responses are extremely important in modeling such phenomena like dilatation or compaction and stress-(or strain-)induced anisotropy for granular materials. Moreover, as can easily be seen from Eqs. (11) and (26), the effect of the intermediate principal stress, σ_2, which is related to the direction of the stress path in the deviatoric plane [12], is accounted for by the inclusion of the third stress invariant $\bar{I}_3$. The importance of these phenomena has

been supported by experimental results, and it is desirable to include them in the mathematical model.

It is a limitation of most elasticity-based models that behavior in unloading is not correctly described; these models are basically intended for use in cases where monotonically increasing loads prevail. Since there is no explicit yield (or loading) surface in the elasticity models, the definition of loading and unloading has no clear cut meanings. This has naturally led to the introduction of loading functions in the theory of plasticity. However, in the present formulation, an approximate method of modeling unloading and reloading behavior will be described and used in the prediction for some tests on sand. Furthermore, a failure condition will be postulated in order to determine the limiting state of stress.

5. Unloading - Reloading Behavior and Failure Condition

5.1 Approximate Modeling of Unloading - Reloading

The observations and studies made in Refs. [8, 10, 15, 28] have shown that unloading and reloading behavior of many soils is very nearly linear and elastic in nature. Further, this behavior is independent of the stress and strain levels at which unloading starts. For example, in conventional triaxial compression tests (Fig. 5), unloading and reloading at different stress levels, A and B, will have essentially the same slope which is nearly the same as the slope of the initial tangent, as shown in Fig. 5. Actual behavior of soils will show a small hysteresis loop as that shown at point A in Fig. 5. Based one these observations, the unloading and reloading (to the maximum previous stress level) is approximated herein as being linear elastic. This behavior is completely described by any two of the familiar elastic moduli (E, ν, K, G, and M).

The values of these two parameters are approximately chosen to be those of the initial tangent moduli. In the following two expressions for the initial tangent Young's modulus, E_i, and Poisson's ratio, ν_i, are developed from the general expressions in the conventional tests.

Considering the expressions given in Eqs. (18) for the CTC test, it can easily be shown that the initial moduli E_i and ν_i are given by:

$$\frac{1}{E_i} = \left[\frac{\partial \Delta\varepsilon_1}{\partial \lambda}\right]_{\lambda=0} = (B_1 + B_4) + (6B_2 + 5B_3 + 2B_5)\sigma_c + (27B_6 + 24B_7 + \frac{5}{2}B_8 + 8B_9)\sigma_c^2 \qquad (29a)$$

and

$$\nu_i = -\left[\frac{\partial \Delta\varepsilon_2}{\partial \Delta\varepsilon_1}\right]_{\lambda=0} = -\left[\frac{\partial \Delta\varepsilon_2}{\partial \lambda}\ \frac{\partial \lambda}{\partial \Delta\varepsilon_1}\right]_{\lambda=0} \quad ; \quad \text{i.e.}$$

$$\nu_i = -\left[\frac{B_1 + (6B_2 + 2B_3)\sigma_c + (27B_6 + 15B_7 + B_8 + 2B_9)\sigma_c^2}{(B_1+B_4) + (6B_2+5B_3+2B_5)\sigma_c + (27B_6+24B_7+\frac{5}{2}B_8+8B_9)\sigma_c^2}\right] \qquad (29b)$$

These expressions will be used in modeling the unloading-reloading behavior. As can be seen from Eqs. (29a, b), both elastic moduli depend on the initial value of the hydrostatic (confining) pressure as has been experimentally demonstrated.

Finally, in order to complete the formulation of the approximate method of modeling the loading-unloading behavior, it is necessary to postulate a loading criterion. In simple test cases, unloading and reloading can be easily visualized from the examination of the stress-strain curves. However, for a completely general case, a clear well-defined criterion for unloading that is the same in any coordinate system (i.e., invariant) is needed. Herein, a simple unloading and reloading condition is used. This condition is expressed in terms of the complementary energy function Ω defined earlier which is invariant with respect to coordinate transformation. Unloading is indicated by the condition $\dot{\Omega} < 0$, where $\dot{\Omega} = \varepsilon_{ij} d\sigma_{ij}$

is the incremental change in Ω. The condition $\dot{\Omega} > 0$ indicates loading. Reloading is defined by the condition $\dot{\Omega} > 0$ and $\Omega < \Omega_{max}$, where Ω_{max} is the maximum previous value of Ω at the material point. Mathematically, these general conditions may be written as:

$$\begin{aligned} &\text{Loading:} \quad \text{when } \Omega = \Omega_{max} \text{ and } \dot{\Omega} > 0 \\ &\text{Unloading: when } \Omega \leq \Omega_{max} \text{ and } \dot{\Omega} < 0 \\ &\text{Reloading: when } \Omega < \Omega_{max} \text{ and } \dot{\Omega} > 0 \end{aligned} \tag{30}$$

For cases of unloading or reloading the moduli of Eqs. (29a, b) apply, while for loading the expressions of Eqs. (26) or (27) are used. In terms of stresses, $\dot{\Omega}$ can be calculated using Eq. (11a) as

$$\dot{\Omega} = \frac{\partial \Omega}{\partial \sigma_{ij}} \dot{\sigma}_{ij} = \phi_1 \dot{\bar{I}}_1 + \phi_2 \dot{\bar{I}}_2 + \phi_3 \dot{\bar{I}}_3 \tag{31}$$

in which the following relations for the increment invariants $\dot{\bar{I}}_1$, $\dot{\bar{I}}_2$ and $\dot{\bar{I}}_3$

$$\dot{\bar{I}}_1 = \dot{\sigma}_{kk} \; ; \quad \dot{\bar{I}}_2 = \sigma_{ij} \dot{\sigma}_{ij} \quad \text{and} \quad \dot{\bar{I}}_3 = \sigma_{im} \sigma_{jm} \dot{\sigma}_{ij} \tag{31a}$$

have been used. The only objection of the present definition of loading and unloading, as for most variable-moduli models, is the ambiguity encountered at the neutral loading condition $\dot{\Omega} = 0$, where one may arbitrarily assign either value of the loading or unloading moduli. The result is that infinitesimal stress changes near neutral loading may produce finite strain changes, and continuity condition may be violated which is not physically acceptable. However, apart from severe multi-dimensional loading conditions, many practical solutions involve moderate loading conditions and loading paths near neutral loading are not likely to occur most often.

5.2 Mohr-Coulomb Failure Condition

For a general practical finite element, a failure condition must be postulated in order to determine the limiting state of stress. For granular materials, different failure conditions have been proposed and used, such as Mohr-Coulomb and Drucker-Prager conditions [3, 9, 24]. Experimental results have shown that Mohr-Coulomb criterion is among the best failure conditions and it yields reasonably accurate results for most soils. Herein, this failure criterion is employed for the three soils described.

In the π- (deviatoric) plane, the Mohr-Coulomb condition is represented by an irregular hexagon, as shown in Fig. 6. The general expression for Mohr-Coulomb condition may be written as [3]:

$$f = \sigma_1(1 - \sin\phi) - \sigma_3(1 + \sin\phi) - 2c\cos\phi = 0 \qquad (32)$$

where σ_1 = the major (max.) principal stress, σ_3 = the minor (min.) principal stress, c = cohesion and ϕ = angle of internal friction of the soils, and soil mechanics sign convention is used (compression is positive). For undrained conditions, effective stresses and effective values for c and ϕ are used.

6. Theoretical Conditions: (Uniqueness and Stability)

It is a desirable feature for any mathematical theory describing the mechanical behavior of materials that the resulting solutions for practical problems are unique and exhibit stable equilibrium configurations. These characteristics are generally to be expected for most actual physical situations. The stability and uniqueness requirements and their implications for elasticity based constitutive models are discussed in Ref. [4], based on Drucker's material stability postulate [10]. The

implications of Drucker's stability postulate on the constitutive relations presented may be summarized in the following:

(1) Although the present formulation is based on an assumed function for Ω, stability postulate assures the existence of the strain energy density function, W such that $W + \Omega = \sigma_{ij}\varepsilon_{ij}$, and the laws of thermodynamics are always satisfied. Moreover, the Hessian matrices [H] and [H'] for both functions W and Ω, respectively, are positive definite, where the components of these matrices are defined as [12]:

$$H_{ijkl} = \frac{\partial^2 W}{\partial \varepsilon_{ij} \partial \varepsilon_{kl}} \quad ; \quad H'_{ijkl} = \frac{\partial^2 \Omega}{\partial \sigma_{ij} \partial \sigma_{kl}} \tag{33}$$

(2) The surfaces W = const. and Ω = const. are always convex in the strain or stress space, respectively.

(3) Based on the positive definite character of the Hessian matrices, the inverse constitutive relations always exist. For example, the inverse relation of Eq. (27) exists and stress increments, $\dot{\sigma}_{ij}$, can always be uniquely determined in terms of the strain increments, $\dot{\varepsilon}_{ij}$. This is an extremely important requirement in the finite element formulation which always requires the material stiffness matrix $[D] = [C]^{-1}$.

Satisfaction of the above requirements can be achieved numerically during the solution process. This will guarantee the uniqueness of the results obtained for each step in incremental finite element solutions.

7. Comparison of Experimental With Theoretical Results

Herein, the numerical results obtained using the proposed model and the determined material constants will be compared to the experimental results used as data base for model formulation. Based on these comparisons and the discussion made earlier, a number of conclusions will be

summarized in the following section.

For clay "X", typical stress-strain curves for some of the loading paths in the tests provided as data base are shown in Fig. 7. Good agreement is obtained between experimental and theoretical results in most of the cases. However, there are some discrepancies between calculated and measured strains for the case of σ_c = 20 psi and m = 1; the model underestimates the axial and lateral strains at high stress levels, as shown in Figs. 7(c) and (d). Considering the volumetric strains observed under constant mean normal stresses, the model correctly predicts volume changes. However, this only qualitatively, since the calculated volumetric strains are too small compared to the measured values, as can be seen from Fig. 7(h). This is expected in the present formulation since the model in its present form cannot account for material initial (inherent) anisotropy which has been observed for clays "X" and "Y". For example, for the case σ_c = 30 psi and m = 0, the model correctly predicts the axial strain, ε_1, and lateral strain, ε_3, but it gives extensional strains for $\varepsilon_2 (= \varepsilon_3)$ while the test measurements indicate compressive values at high stress levels. Obviously, this causes reduction in the calculated values for ε_v.

Comparison of the experimental with theoretical stress-strain curves for clay "Y" are illustrated in Fig. 8 for some of the tests provided. Again, a reasonably good overall agreement is observed in most cases. Unlike clay "X", the measured values of ε_v for clay "Y" are small, and the model reproduces them with a better agreement with the test results, as shown in Figs. 8(b), (d) and (f). As for clay "X", the calculated values for the lateral strains, ε_2, do not agree with the experimental results in many cases because of the initial anisotropy exemplified previously.

Different comparisons of the measured and calculated stress-strain curves for Ottawa sand are made in Fig. 9. The results in the CTE and TE tests, Figs. 9(a) to (d), are in good agreement with the measured values, both in terms of the axial and lateral strains. In the CTC tests, the discrepancies are more pronounced. Although, the initial soil behavior, at low stress levels, appears to be adequately represented by the model, the test data depart significantly from the calculated curves for large stress levels, particularly for the case σ_c = 5 psi, as shown in Figs. 9(g) and (h). However, the overall agreement for the cases shown and those which are not included here is reasonably good. Also, the approximate modeling of loading-unloading behavior is seen to be adequate, as can be observed in Figs. 9(c) and (d). The predicted failure stresses using Mohr-Coulomb condition agree very well with the test values, as can be seen in Figs. 9(e) and (g), for example. In Ref. [20], other cases were investigated using the same values of the material constants employed here, and good agreement with experiments was obtained (in the cases reported in [23], stress-strain curves were shown only for low stress levels below the failure values). Hence, based on the cases investigated both in Ref. [23] and in the present paper, it is believed that the values of the constants used will give the best results at low stress levels compared to the failure values.

In order to study the effect of the change in the values of the material constants on the behavior of the model, comparison is made in Fig. 10 for the two sets of constants given in sec. 3. The results shown are for a proportional loading stress path with $\Delta\sigma_x : \Delta\sigma_y : \Delta\sigma_z$ = 0.5 : 0.5 : 1, and σ_c = 10 psi. The results shown indicate that the behavior of the model becomes sensitive to changes in the constants as the stress

level increases, and completely different results are obtained. This will be more pronounced for increasing proportional loading paths where large stress levels are generally expected before failure (e.g., near HC path). However, the strains occurring in stress paths near the HC path are generally small compared to those observed under most other loading conditions in practical engineering problems so that discrepancies of the results for these loading conditions may be less significant to overall soil behavior than discrepancies in other stress paths. The important point to make is that it is necessary to appreciate the conditions under which the model will be used, and to determine the material constants from tests performed under conditions selected to duplicate as many as possible of the expected field conditions.

8. Summary and Conclusions

The formulation of nonlinear hyperelastic constitutive model, originally developed by Ko and Masson [23], has been presented and applied to three different types of soils: clays "X" and "Y", and Ottawa sand. Detailed description of the procedure of determining the nine material constants in the model has been made and the stress-strain relations for general straight line stress paths and for examples of stress paths in conventional soil tests are given. Incremental forms of the constitutive relations, approximate method of modeling unloading-reloading behavior, and a failure condition are also included for general nonlinear finite element analyses. Finally, comparisons of the results obtained with the experimental measurements are made.

Against the background of the discussion and comparisons made in the present study, the following conclusions, concerning the advantages and limitations of the proposed procedures, can be made:

(1) The proposed constitutive relations can model many of the characteristics of soil behavior such as: nonlinearity, stress-path dependency, dilatation, stress-induced anisotropy, effect of the confining (or hydrostatic) stress, the effect of the third stress invariant, and the noncoincidence of the principal axes of stress and strain increment tensors, especially near failure. However, the present formulation is limited to initially isotropic materials.

(2) When used for monotonically increasing loading conditions, the present formulation satisfies all the rigorous mathematical requirements such as uniqueness, stability and continuity. For cases where general unloading-reloading conditions are expected, the present approximate criterion proposed for loading and unloading fails to satisfy the continuity condition at or near neutral loadings. Further refinement is needed concerning this aspect.

(3) Once the nine material constants are determined, the incremental form of the model can be easily implemented in finite element codes for general analyses. The method described for material constants determination allows a great flexibility for inclusion as many test data as possible in the fitting procedure. However, the procedure is not easy to apply; many trials for fitting the cubic curves may be needed in order to obtain reasonable results.

(4) For the cases investigated, the model gives a reasonably good overall agreement with the experimental results for the tests used as data base in the model formulation. But the model fails to predict the large volumetric strains for clay X, and the behavior near failure for Ottawa sand in CTC and TC tests. For almost all of the cases studied, the model does not correctly predict the values of the principal strain ε_2 for

clays "X" and "Y". This is expected because of the initial anisotropy observed for both soils which cannot be accounted for in the present formulation.

(5) The model behavior for Ottawa sand is found to be sensitive to changes in values of the material constants for increasing proportional loading stress paths where large stress levels are generally expected before failure. Duplication of as many expected field conditions as possible in the tests used for model calibration is generally recommended to reduce such effects.

(6) Best results from the model are generally expected at low stress levels below failure. This is usually the range where most of the elasticity-based models are frequently used.

(7) The present formulation cannot account for post-failure behavior in strain-softening materials (e.g., dense sand) since it indicates increasing strains for increasing stresses (work-hardening type).

Acknowledgments

This material is based upon work supported by the National Science Foundation under Grant No. PFR-7809326 to Purdue University.

References

1. Chang, T. Y., et al., "An Integrated Approach to Stress Analysis of Granular Materials," Lab. Report, California Institute of Technology, Soil Mechanics Laboratory, 1967.

2. Chen, W. F., "Plasticity in Soil Mechanics and Landslides," Journal of the Engineering Mechanics Division, ASCE, vol. 106, no. EM3, June, 1980, pp. 443-464.

3. Chen, W. F., Limit Analysis and Soil Plasticity, Scientific Publishing Publishing Co., Elsevier, Amsterdam, The Netherlands, 1975.

4. Chen, W. F., and Saleeb, A. F., "Constitutive Equations for Engineering Materials," vol. 1. "Elasticity and generalized stress-strain models." Lecture Notes in Structural Engineering, School of Civil Engineering, Purdue University, West Lafayette, Indiana, 1980.

5. Clough, R. W., and Woodward, R. J. III, "Analysis of Embankment Stress and Deformations," Journal of Soil Mechanics and Foundations Division, ASCE, vol. 93, no. SM4, July, 1967, pp. 529-549.

6. Coon, M. D., and Evans, R. J., "Recoverable Deformation of Cohesionless Soils," Journal of the Soil Mechanics and Foundations Division, ASCE, vol. 97, no. SM2, Feb., 1971, pp. 375-391.

7. Corotis, R. B., Frazin, M. H., and Krizek, R. J., "Nonlinear Stress-Strain Formulation for Soils," Journal of the Geotechnical Engineering Division, ASCE, vol. 100, No. GT9, Sept., 1974, pp. 993-1008.

8. Domaschuk, L., and Wade, N. H., "A Study of Bulk and Shear Moduli of Sand," Journal of the Soil Mechanics and Foundations Divison, ASCE, vol. 95, no. SM2, March, 1969, pp. 561-582.

9. Drucker, D. C., and Prager, W., "Soil Mechanics and Plastic Analysis or Limit Design," Quarterly of Applied Mathematics, vol. 10, no. 2, 1963, pp. 157-165.

10. Drucker, D. C., "A More Fundamental Approach to Plastic Stress-Strain Relations," Proceedings, 1st U.S. National Congress on Applied Mechanics, 1951, pp. 487-491.

11. Duncan, J. M., "Finite Element Analyses of Stresses and Movements in Dams, Excavation and Slopes," Proc. Symposium on Applications of the Finite Element Method in Geotechnical Engineering, Vicksburg, Mississippi, USA, May, 1972, pp. 267-326.

12. Duncan, J. M., and Chang, C-Y, "Nonlinear Analysis of Stress and Strain in Soils," Journal of the Soil Mechanics and Foundations Division, ASCE, vol. 96, no. SM5, September, 1970, pp. 1629-1653.

13. El-Sohby, M. A., "Deformation of Sands Under Constant Stress Ratios," Proc. of the 7th Int. Conference on Soil Mechanics and Foundation Engineering, Int. Soc. of Soil Mechanics and Foundation Engineering, vol. 1, 1969, pp. 111-119.

14. El-Sohby, M. A., "Elastic Behavior of Sand," Journal of the Soil Mechanics and Foundations Division, ASCE, vol. 95, no. SM6, Nov., 1969, pp. 1393-1409.

15. Eringen, A. C., Nonlinear Theory of Continuous Media, McGraw-Hill Book Co. Inc., New York, N.Y., 1962.

16. Evans, R. J., and Pister, K. S., "Constitutive Equations for a Class of Nonlinear Elastic Solids," International Journal of Solids and Structures, vol. 2, no. 3, 1966, pp. 427-445.

17. Girijavallabhen, C. V., and Reese, L. C., "Finite Element Method for Problems in Soil Mechanics," Journal of the Soil Mechanics and Foundations Divison, ASCE, vol. 94, no. SM2, March, 1968, pp. 473-496.

18. Hardin, B. O., "The Nature of Stress-Strain Behavior for Soils," State-of-the-Art Report for the ASCE Specialty Conference on Earthquake Engineering and Soil Dynamics, Pasadena, California, Proceedings, vol. 1, June, 1978, pp. 3-90.

19. Holubec, I., "Elastic Behavior of Cohesionless Soil," Journal of the Soil Mechanics and Foundations Divison, ASCE, vol. 94, no. SM6, Nov., 1968, pp. 1215-1231.

20. Janbu, N., "Soil Compressibility as Determined by Oedometer and Triaxial Tests," Proceedings, European Conference on Soil Mechanics and Foundation Engineering, Wiesbaden, Germany, vol. 1, 1963, pp. 19-25.

21. Ko, H. Y., and Scott, R. F., "Deformations of Sand in Hydrostatic Compression," Journal of the Soil Mechanics and Foundations Division, ASCE, vol. 93, no. SM3, May, 1967, pp. 137-156.

22. Ko, H. Y., and Scott, R. F., "Deformation of Sand in Shear," Journal of the Soil Mechanics and Foundations Divison, ASCE, vol. 93, no. SM5, Sept., 1967, pp. 283-310.

23. Ko, H. Y., and Masson, R. M., "Nonlinear Characterization and Analysis of Sand," Numerical Methods in Geomechanics, ASCE, 1976, pp. 294-305.

24. Lade, P. V., "The Stress-Strain and Strength Characteristics of Cohesionless Soils," Thesis presented to the University of California at Berkeley, in 1972, in partial fulfillment of the requirements for the degree of Doctor of Philosophy.

25. Makhlouf, H. M., and Stewart, J. J., "Factors Influencing the Modulus of Elasticity of Dry Sand," Proceedings, 6th International Conference on Soil Mechanics and Foundations Engineering, Montreal, vol. 1, 1965, pp. 298-302.

26. Nelson, I., and Baladi, G. Y., "Outrunning Ground Shock Computed with Different Models," Journal of the Engineering Mechanics Division, ASCE, vol. 103, no. EM3, June, 1977, pp. 377-393.

27. Nelson, I., and Baron, M. L., "Application of Variable Moduli Models to Soil Behavior," Int. Journal of Solids and Structures, vol. 7, 1971, pp. 399-417.

28. Romano, M., "A continuum Theory for Granular Media with a Critical State," Archives of Mechanics, vol. 26, no. 6, 1973, pp. 1011-1028.

29. Scott, R. F., and Ko, H. Y., "Stress Deformation and Strength Characteristics," Proceedings of the 7th Int. Conference on Soil Mechanics and Foundation Engineering, International Society for Soil Mechanics and Foundation Engineering, vol. 1, 1969, pp. 1-49.

30. Smith, I. M., and Kay, S., "Stress Analysis of Contractive or Dilative Soil," Journal of the Soil Mechanics and Foundations Division, ASCE, vol. 97, no. SM7, July, 1971, pp. 981-997.

31. Truesdell, C., "Hypo-elasticity," Journal of Rational Mechanics and Analysis, vol. 4, no. 1, 1955, pp. 83-133.

32. Vagneron, J., Lade, P. V., and Lee, K. L., "Evaluation of Three Stress-Strain Models for Soils," Numerical Methods in Geomechanics, ASCE, 1976, pp. 1329-1351.

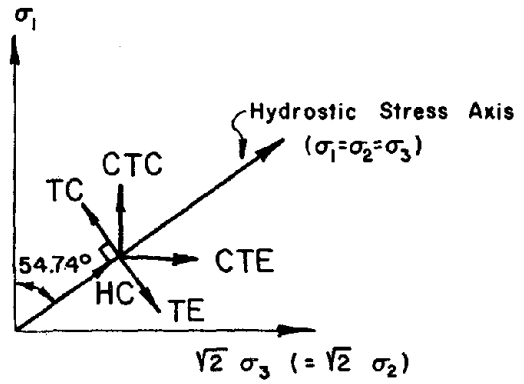

(a) Stress Paths in the Triaxial Stress Plane

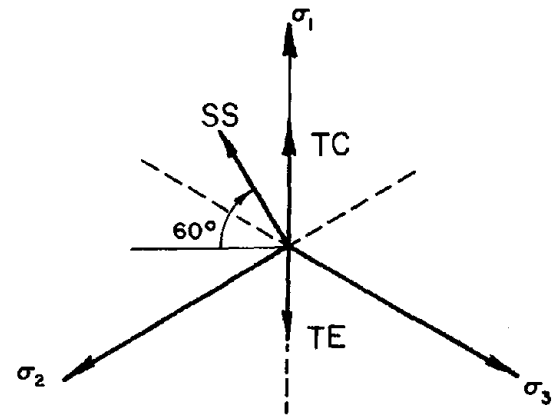

(b) Stress Paths in the Deviatoric (π-) Plane

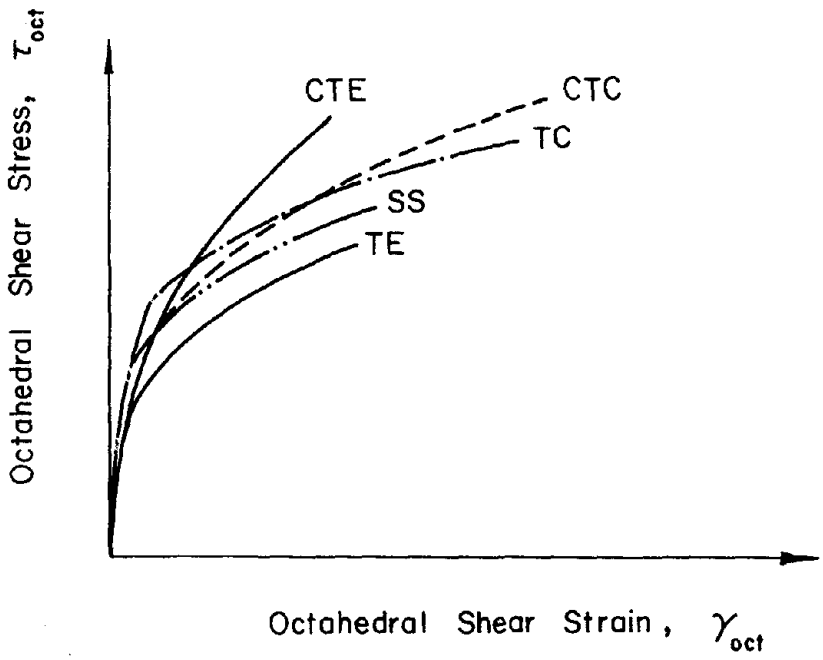

(c) Octahedral Shear Stress-Strain Curves

FIG 1. Typical Octahedral Shear Stress-Strain Curves for Ottawa Sand for Different Stress Paths.

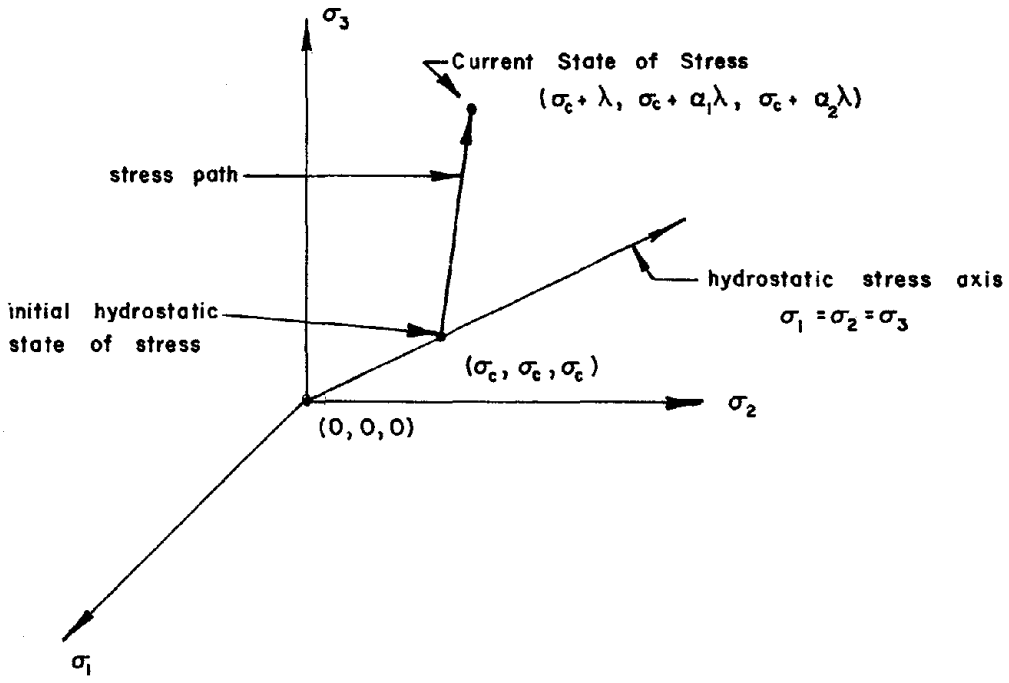

FIG 2. General Straight Line Stress Path in Principle Stress Space.

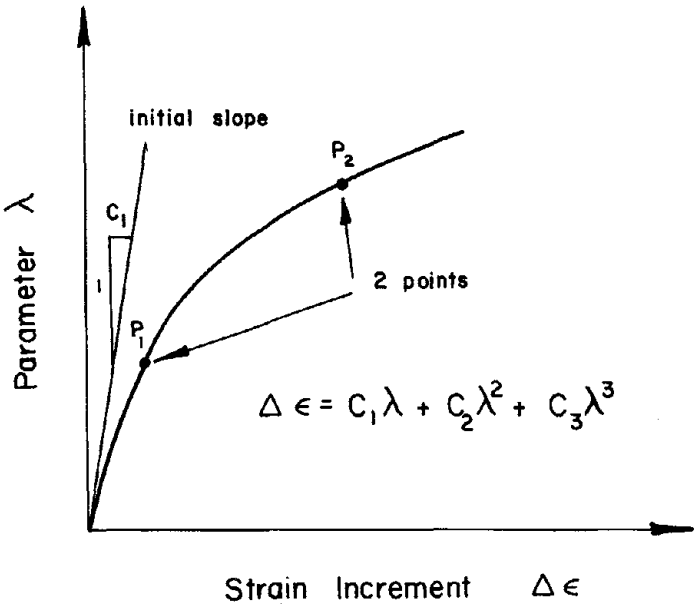

FIG 3. Fitting Procedure for Cubic Curves

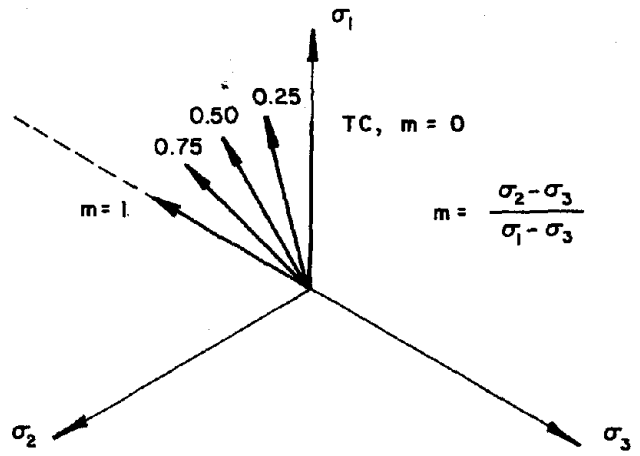

(a) Clay "X"

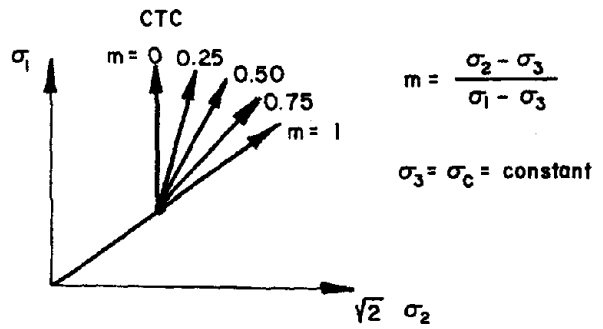

(b) Clay "Y"

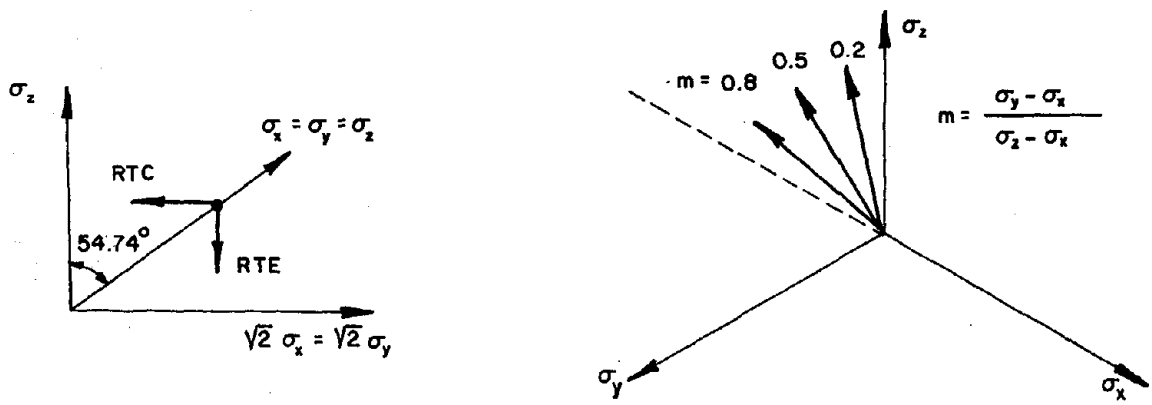

(c) Ottawa Sand

FIG 4. Stress Paths for Prediction for Clay "X", Clay "Y" and Ottawa Sand.

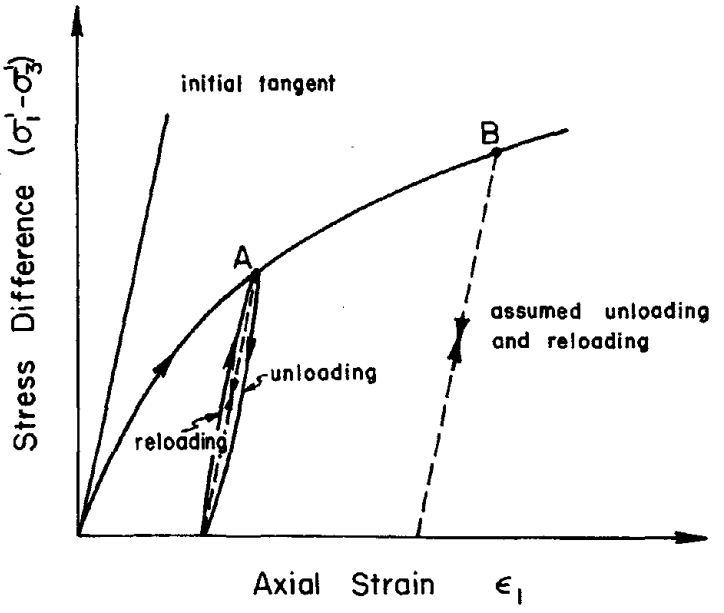

FIG 5. Approximate Representation of Loading-Unloading Behavior in Conventional Triaxial Compression Test

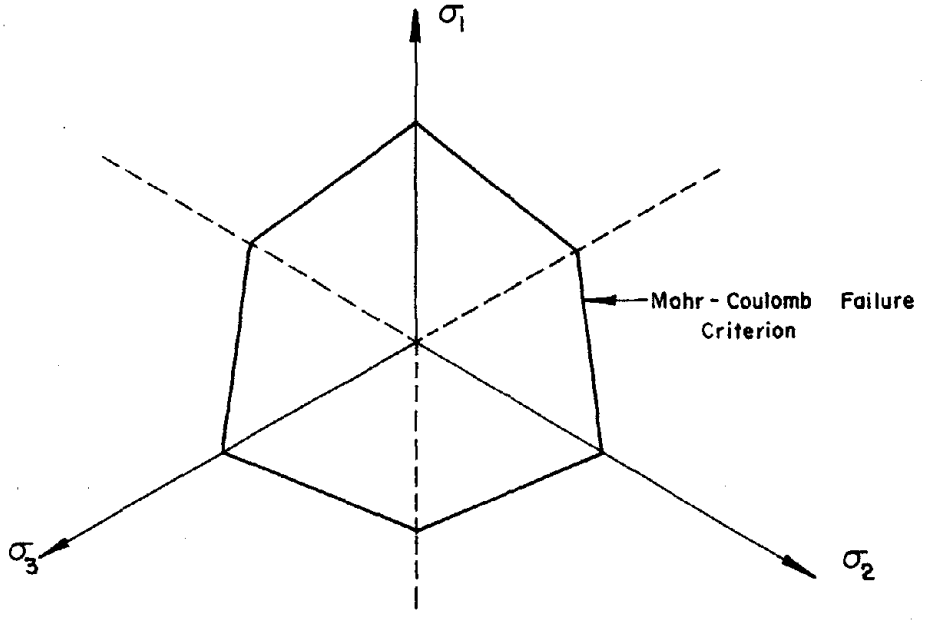

FIG 6. . Mohr-Coulomb Failure Criterion in the Deviatoric Plane

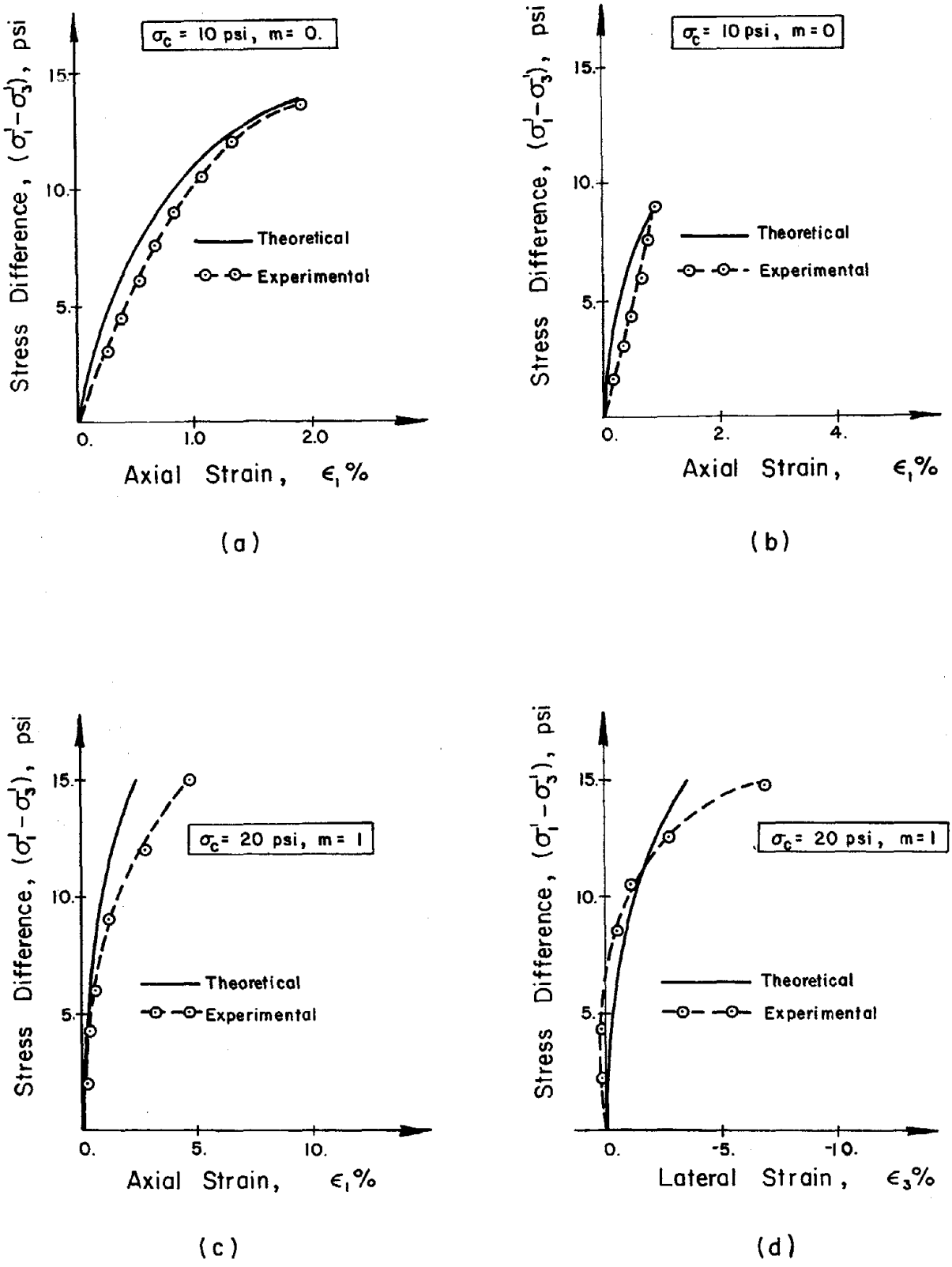

FIG 7. Comparison of Theoretical and Experimental Stress-Strain Curves For Clay "X", (TC Tests with Const. Mean Normal Stress)

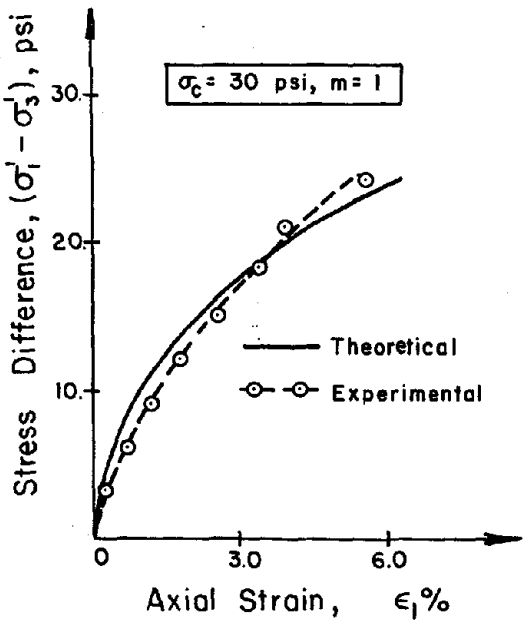

(e)

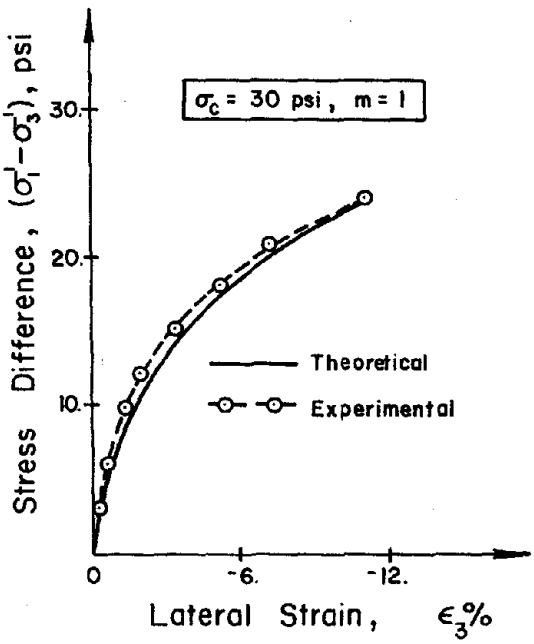

(f)

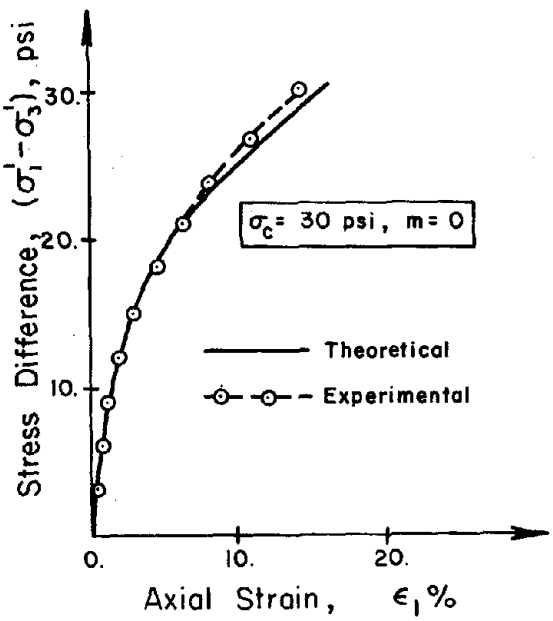

(g)

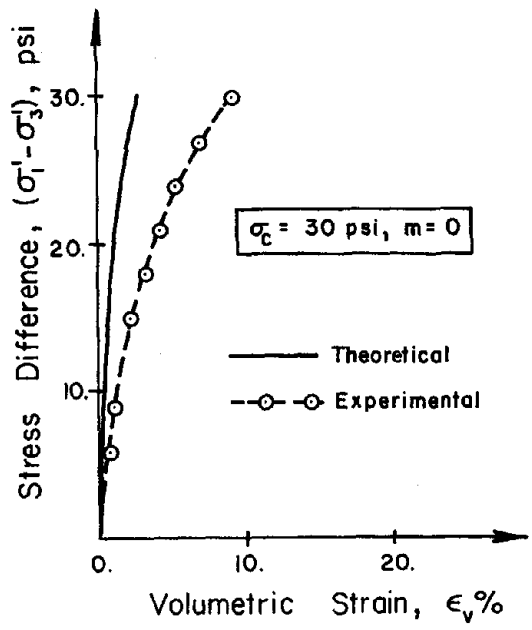

(h)

FIG 7. (Cont'd)

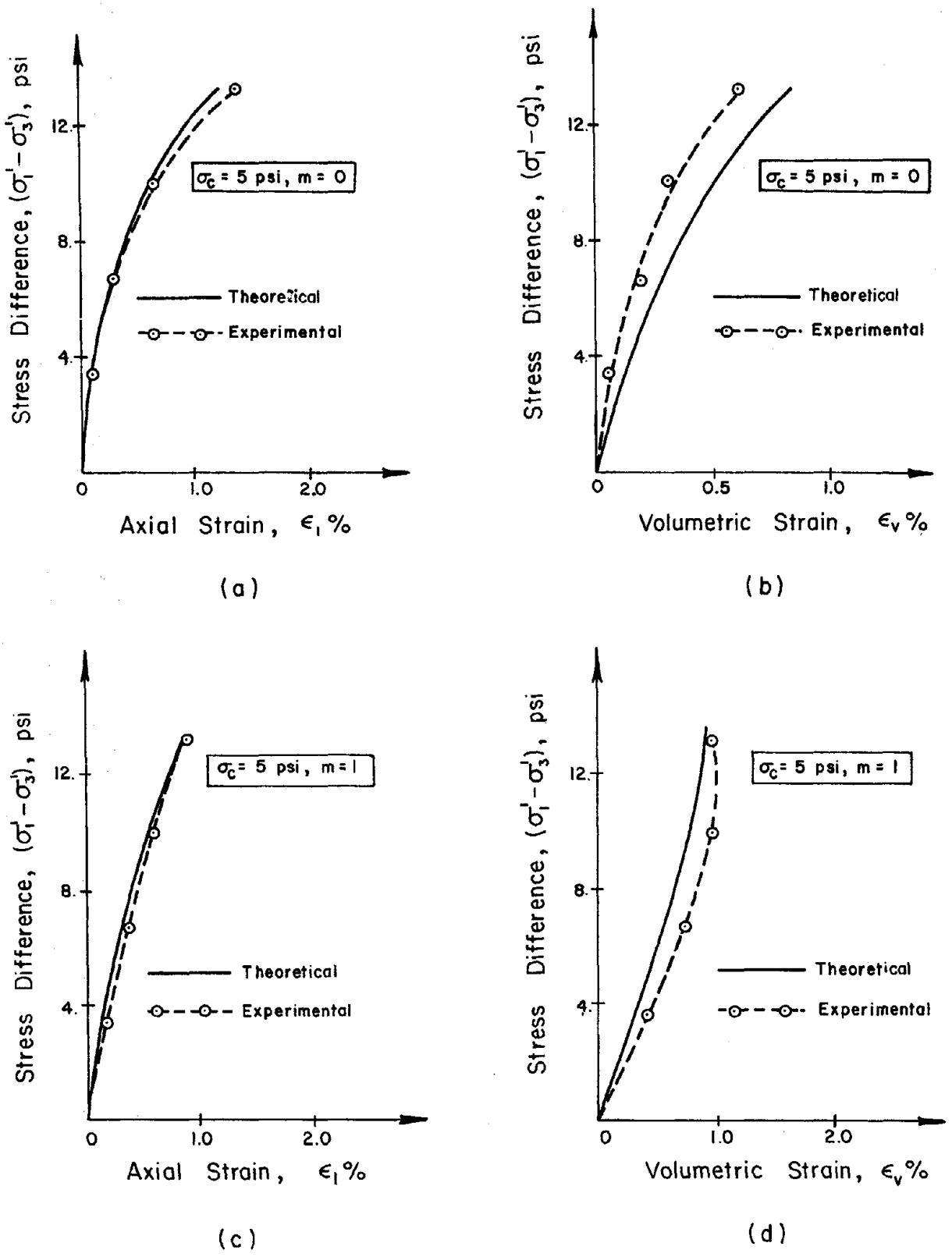

FIG 8. Comparison of Theoretical and Experimental Stress-Strain Curves for Clay "Y", (CTC Tests)

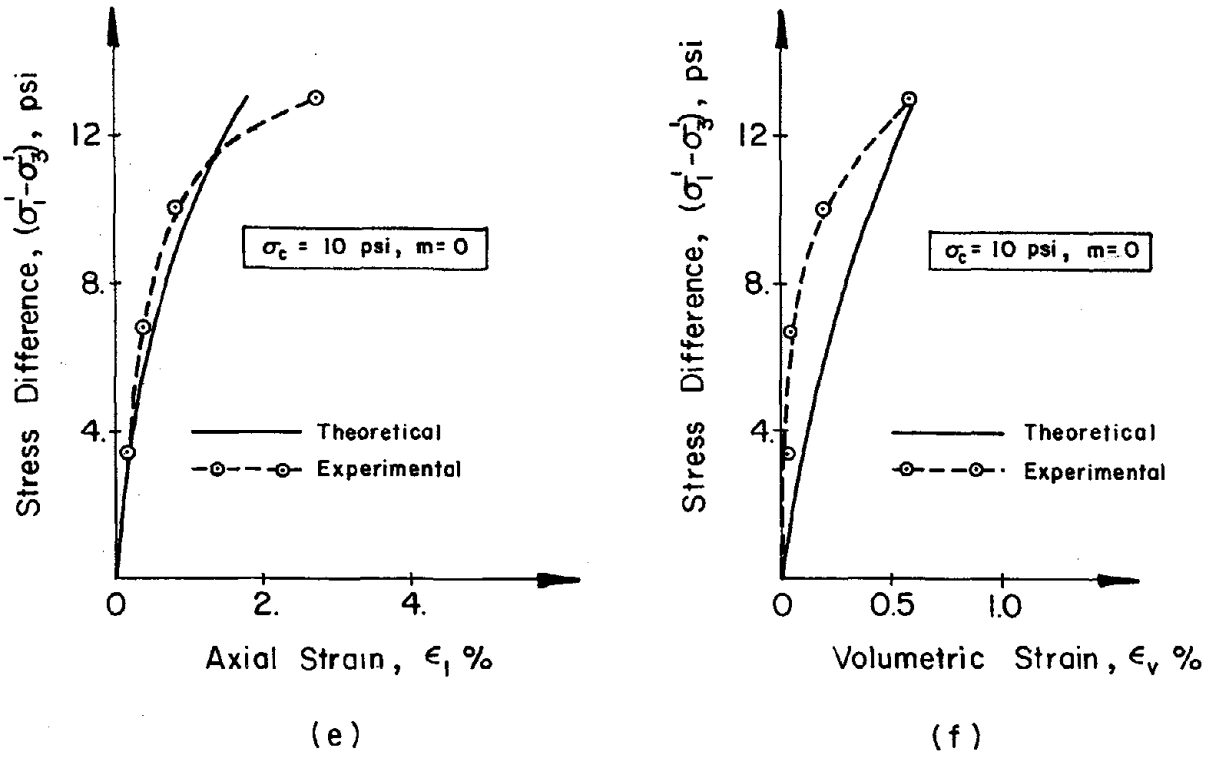
Stress Difference, $(\sigma_1'-\sigma_3')$, psi
12
8.
4.
σ_c = 10 psi, m= 0
Theoretical
Experimental
0
2.
4.
Axial Strain, ϵ_1 %
(e)
Stress Difference, $(\sigma_1'-\sigma_3')$, psi
12
8.
4.
σ_c = 10 psi, m= 0
Theoretical
Experimental
0
0.5
1.0
Volumetric Strain, ϵ_v %
(f)

FIG 8. (Cont'd)

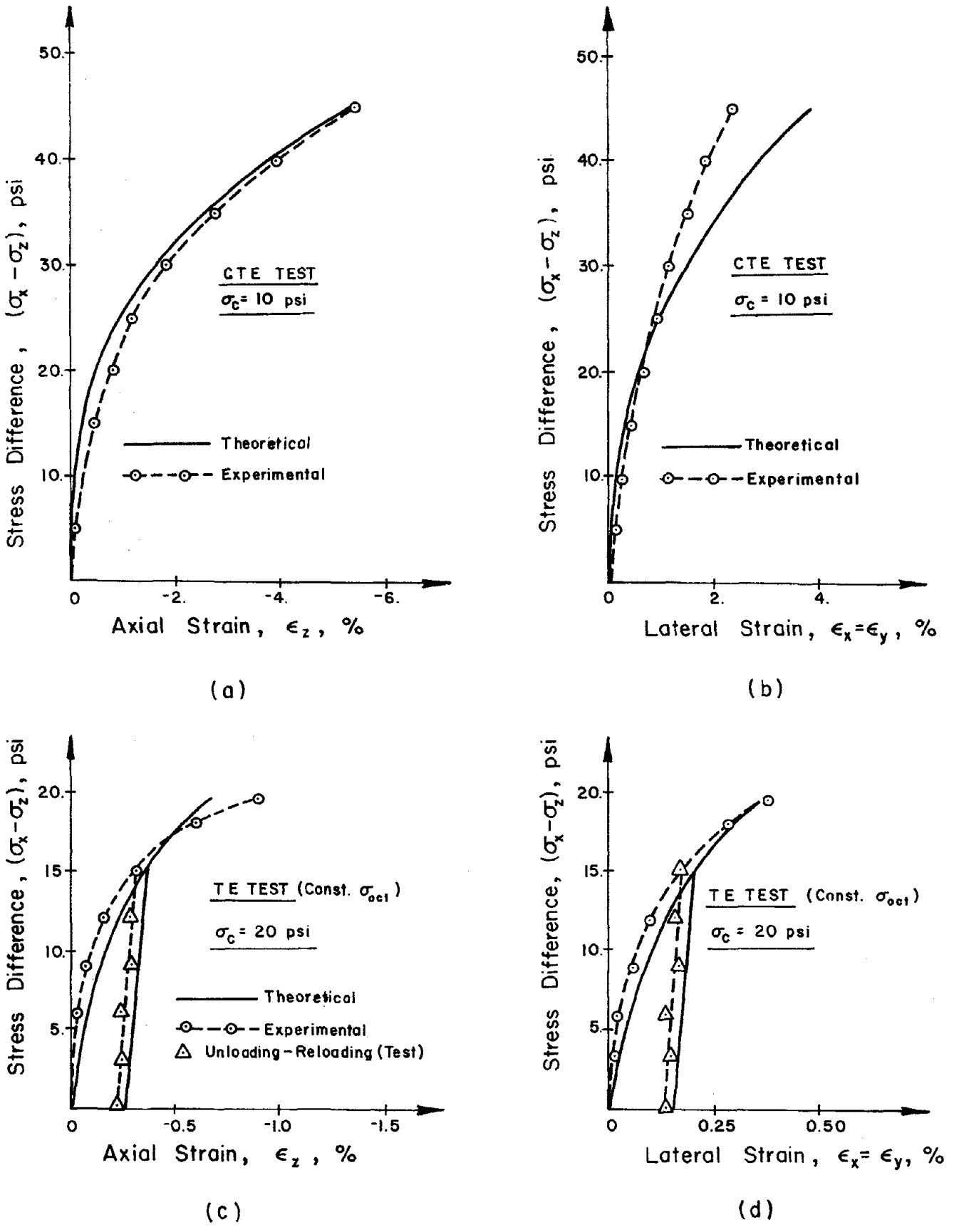

FIG 9. Comparison of Theoretical and Experimental Stress-Strain Curves for Ottawa Sand.

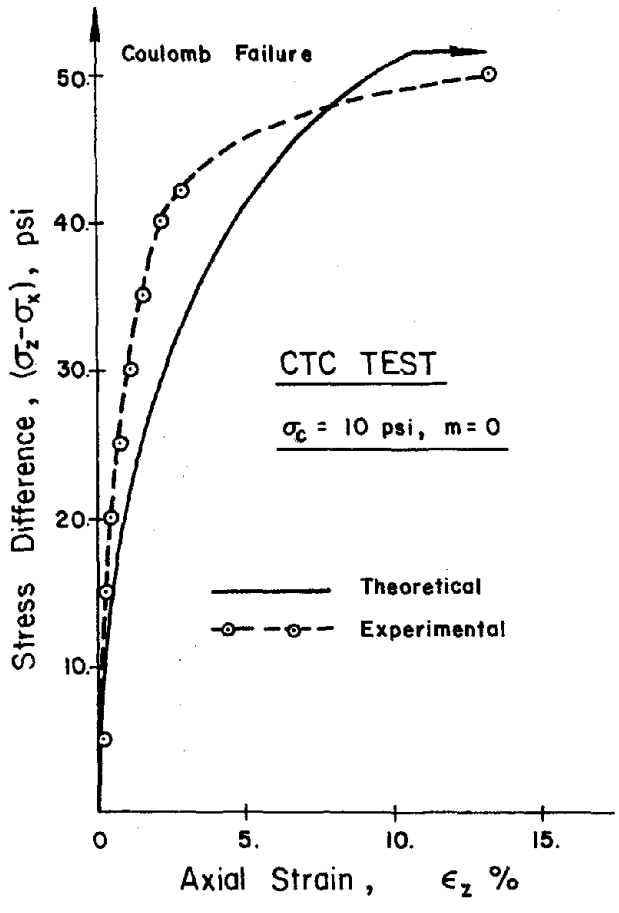

(e)

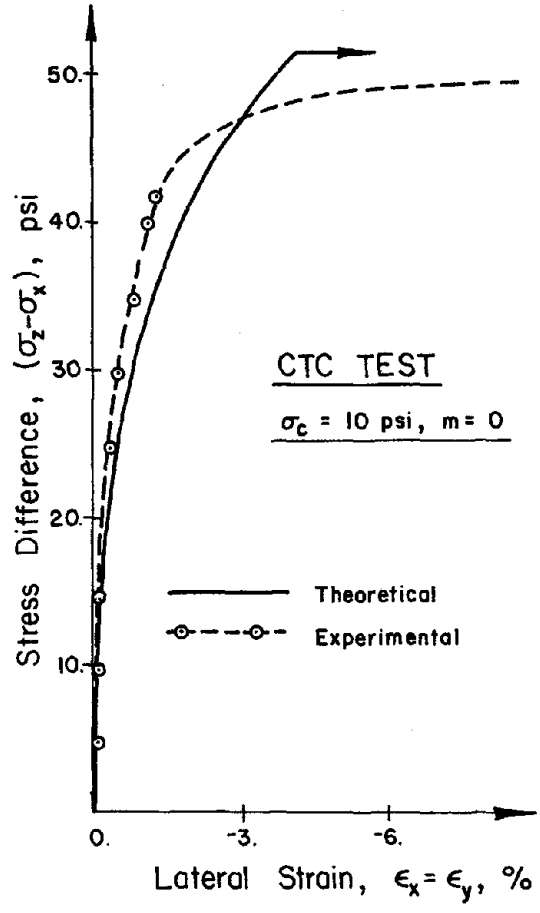

(f)

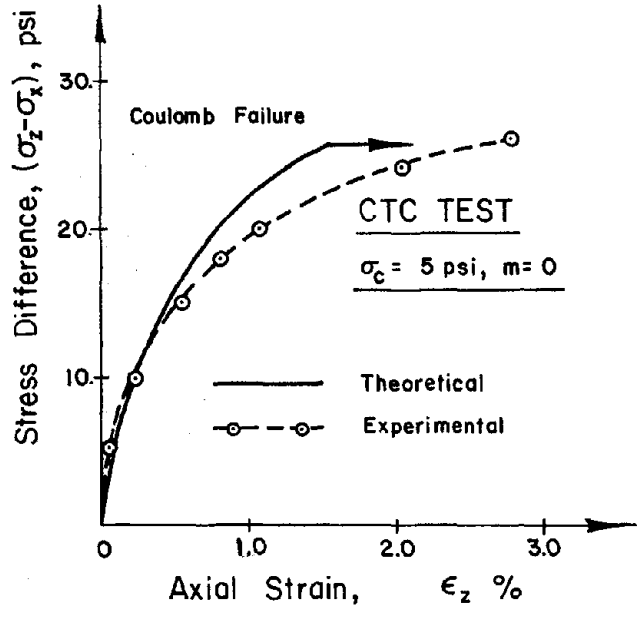

(g)

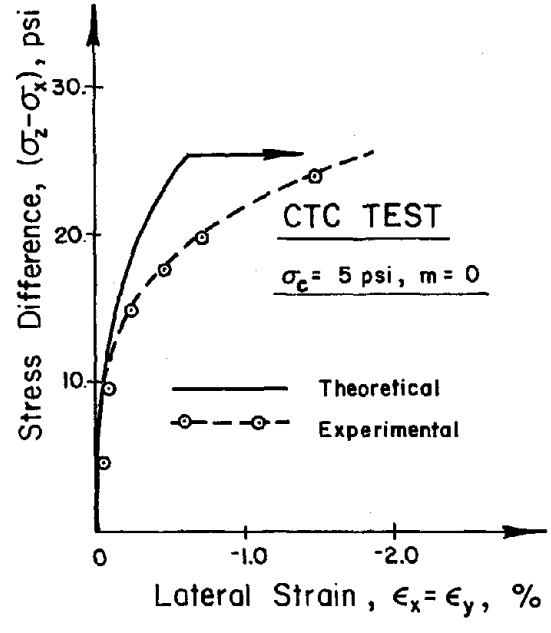

(h)

FIG 9. (Cont'd)

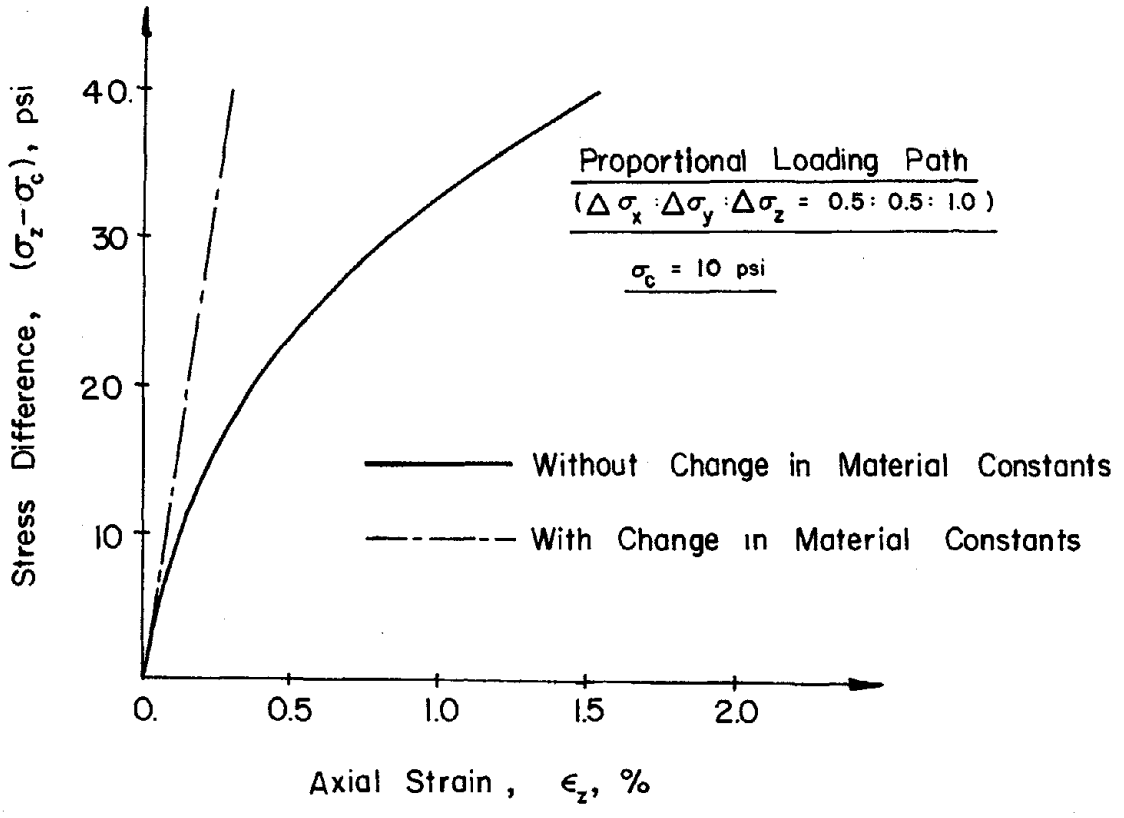

FIG 10. Effect of Changes in Material Constants on the Model Behavior in Proportional Loading Path for Ottawa Sand

List of Figures

Nonlinear Hyperelastic (Green) Constitutive Models for Soils: Predictions and Comparisons

By: A. F. Saleeb and W. F. Chen

School of Civil Engineering

Purdue University

West Lafayette, IN

1. Introduction

In the first part of the present paper (theory and calibration), the formulation of a third-order nonlinear elastic constitutive model based on Green type of formulation has been given, and the model was used to describe the behavior of three different soils: clays "X", "Y" and Ottawa sand. For the different stress paths used in determining the material constants in the model, the theoretical and experimental results have been compared. Based on these comparisons, it was found that the model qualitatively gives good overall fit to the test results; it produces essentially most of the important features of the behavior observed experimentally such as nonlinearity, stress-path dependency, dilatation, stress-induced anisotropy, effect of the intermediate principal stress and the hydrostatic stress, etc. Quantitatively, the agreement between the calculated and the measured values is reasonably good. However, the theoretical model fails to predict the initial anisotropy observed in tests for clays "X" and "Y". Moreover, the model underestimated the volumetric strains for clay X. For Ottawa sand, it has been demonstrated that the model behavior is very sensitive to changes in the higher order material constants in loading paths near hydrostatic stress path when

large stress levels are generally encountered.

Herein, comparisons of the predicted theoretical and experimental results are given for the three soils along test stress paths different from those used in the determination of the material constants in the model. This provides the necessary verification of the applicability of the constitutive model in describing the soil behavior under general three-dimensional states of stress. In the forthcoming, a summary of the comparisons and a number of conclusions will be given for the three types of soils investigated.

2. Comparisons of Theoretical and Experimental Results

(a) Clay "X"

The calculated and measured stress-strain curves along the different stress paths unsed in the prediction for clay "X" are shown in Fig. 1(a) to (p). By examining these curves, the following conclusions may be made:

1. In almost all the cases investigated, good qualitative agreement is observed between the theoretical and the test results, except for the volumetric strains in the case σ_c = 10 psi, m = 0.25, where the model indicates compressive strains while the test gives extensional values, as illustrated in Fig. 1(b).

2. As for the stress paths used in determining the material constants, the model underestimates the volumetric strains in all the cases, and the values of the intermediate principal strain, ε_2, are not correctly predicted. This is mainly due to the inability of the model to take into account the effect of initial anisotropy observed experimentally.

3. In general, the theoretical stress-strain curves for the axial strain ε_1 show stiffer behavior than that of the measured ones, particularly

at low stress levels. The most pronounced discrepancies between the calculated and the test results are observed for σ_c = 10 psi, m = 0.5; and for σ_c = 20 psi, m = 0.25 and 0.5, where the stiffer behavior extends up to the failure stress levels. However, for these cases, the lateral strains, ε_3, agree well with the measured values, as shown in Figs. 1(d) and (j), for example.

4. For the axial strains, ε_1, the best agreement is obtained for the cases of σ_c = 30 psi, and for σ_c = 10 psi, m = 0.25, where the maximum discrepancy is approximately 30%.

5. In almost all the cases, Mohr-Coulomb failure criterion provides reasonably good predictions for failure stresses.

(b) Clay "Y"

Based on the comparisons of the predicted theoretical and experimental stress-strain curves illustrated in Figs. 2(a) to (r), the following conclusions can be made:

1. As for clay "X", good overall qualitative fit is obtained in most cases, However, the predicted values for the volumetric strains, ε_v do not agree, even qualitatively, with the laboratory results for the cases: σ_c = 2.5 psi, m = 0.75; σ_c = 5 psi, m = 0.25; and σ_c = 10 psi, m = 0.5, specially for σ_c = 10 psi, m = 0.5 where the model shows dilatant behavior near failure which is not observed in the test data, as given in Fig. 2(p).

2. The volumetric strains for all other cases are better predicted than those of clay "X", as shown in Figs. (b), (j) and (n), for example.

3. In most cases, the axial strain values are well predicted at low stress levels below failure, except possibly for σ_c = 2.5 psi, m = 0.25, where the theoretical curve is stiffer than the experimental one.

As the stresses increase approaching failure levels, the discrepancies increase. The most notable discrepancy is observed for σ_c = 10 psi, m = 0.75, Fig. 2(q).

4. Because of the initial isotropy of the present model, the calculated values of the intermediate principal strain, ε_2, do no agree with the test results in many cases, as was the case for clay "X", since test data showed strong initial anisotropy for both clays "X" and "Y".

5. The accuracy of Mohr-Coulomb condition in predicting failure stresses for clay "Y" is not as good as for clay "X". For instance, the error in calculated value for σ_1' at failure in the case σ_c = 10 psi, m = 0.75 is approximately 11%. This is mainly because Mohr-Coulomb criterion does not take into account the effect of the intermediate principal stress, σ_2', on failure.

(c) Ottawa Sand

In Figs. 3 to 8, the results of the comparisons for Ottawa sand are illustrated. The curves are plotted in terms of the octahedral shear stress, $\tau_{oct.} = \sqrt{\frac{2}{3} J_2}$, where $J_2 = \frac{1}{2} s_{ij} s_{ij}$ is the second invariant of the stress deviator tensor, s_{ij}. The following observations and conclusions may be made:

1. Reasonably good overall qualitative fit is observed in all cases investigated except for the small compressive lateral strains $\varepsilon_x = \varepsilon_y$ observed experimentally in RTC test at low stress levels. Quantiatively, the predicted values for the SS tests with $\sigma_{oct.}$ = 5 and 10 psi agree well with the test results at low stress levels. At high stress levels near failure, the calculated strains are too small compared to the measured values. For the SS test with σ_{oct} = 20 psi and m = 0.5, the theoretical curves are too soft compared to the experimental curves, as

shown in Figs. 5(a) and (b). The axial strain, ε_z, is better predicted in the RTC test than in the RTE test. However, better agreement is obtained for the lateral strains, $\varepsilon_x = \varepsilon_y$, in the RTE test, Figs. 7 and 8.

2. Although only an approximate modeling of unloading-reloading behavior has been used, the calculated slopes describing the unloading-reloading behavior agree well in most cases with those determined experimentally, as shown in Figs. 3, 4, 5, 6 and 8, for example.

3. The calculated values of failure stresses using Mohr-Coulomb condition are less accurate for Ottawa sand for the stress paths described in Figs. 3 to 8 than for those used in determining the material constants. The theoretical values underestimate the measured failure stresses. In general, the accuracy of predicting failure stresses is less for Ottawa sand than for clays "X" and "Y".

4. At high stress levels in increasing proportional loading stress paths (particularly near HC path), the model predicts very large values of strains compared to those obtained in the actual tests. This can be directly seen from the general expressions of strains in Eq. (16a) in the first part of the paper; although the coefficients of the quadratic and cubic terms, C_2 and C_3, respectively, are generally small for such stress paths, the results obtained are considerably large when these coefficients are multiplied by large values of the parameter λ. As has been shown in Fig. 10 in the first part, the model becomes sensitive to changes in the higher order material constants for large values of λ. The behavior of the model with the changed values of B_6 and B_7 agrees better with the test results provided than the behavior when using the original set of the material constants. The latter greatly overestimates the strain values at high stress levels. More work and further refinement

are needed in determining the material constants to overcome this difficulty.

3. Summary

The formulation of an isotropic third-order hyperelastic constitutive model has been given, and the model has been applied to three types of soil. Theoretical and experimental stress-strain curves were compared for different stress paths for each of the three soils. It was found that the model is capable of describing most of the salient features of soil stress-strain behavior such as nonlinearity, stress-path dependency, dilatation, stress-induced anisotropy, effect of the hydrostatic stress, and the effect of intermediate principal stress and third stress invariant. For monotonically increasing loading conditions, the model satisfies all the rigorous mathematical requirements such as uniqueness, stability and continuity. Reasonably good overall fit has been obtained in most of the cases investigated. However, for clays "X" and "Y", the initial anisotropy observed experimentally cannot be predicted since the present model is initially isotropic. Moreover, it has been found that for Ottawa sand the model, as presently formulated, may exhibit questionable behavior in stress paths near hydrostatic compression stress path where large stress levels are generally encountered. This is mainly because of the large effects of the higher order terms in the constitutive law. More refinement and adjustment of the material constants in the model are needed in order to reduce these effects.

Acknowledgments

This material is based upon work supported by the National Science Foundation under Grant No. PFR-7809326 to Purdue University.

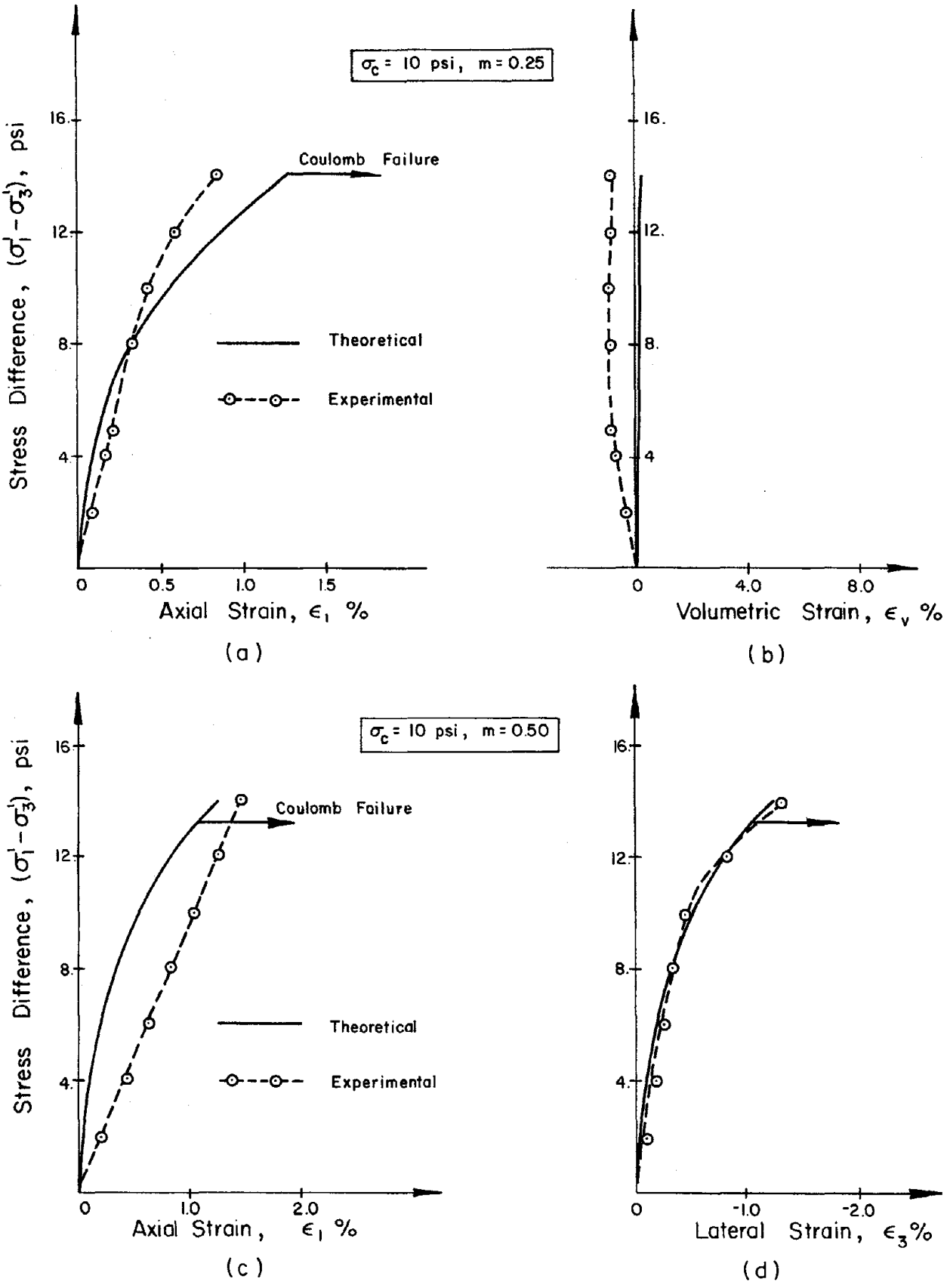

FIG 1. Comparison of the Predicted Theoretical and Experimental Stress-Strain Curves for Clay "X" (TC Tests with Constant Mean Normal Stress)

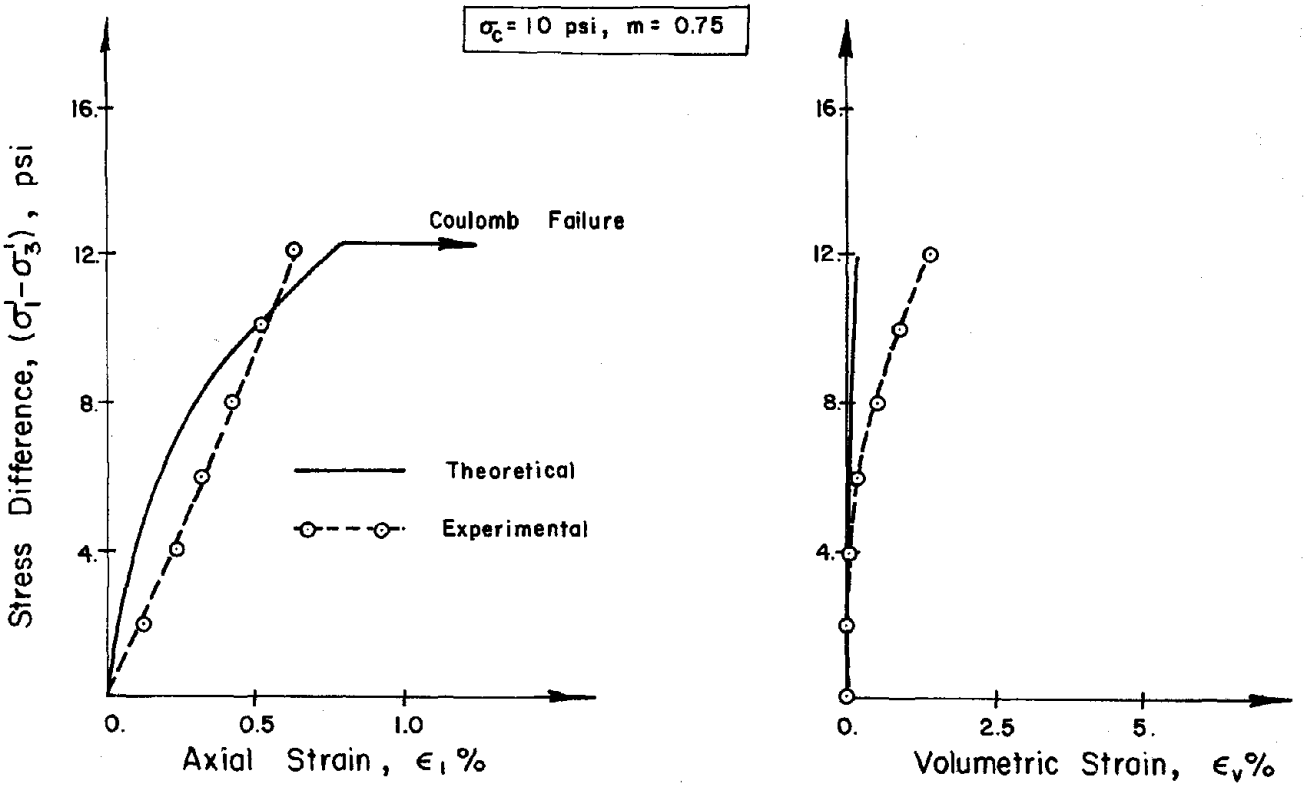
σ_c = 10 psi, m = 0.75
Stress Difference, $(\sigma_1'-\sigma_3')$, psi
16.
12.
8.
4.
Coulomb Failure
Theoretical
Experimental
0.
0.5
1.0
Axial Strain, ϵ_1 %
(e)
16.
12.
8.
4.
0.
2.5
5.
Volumetric Strain, ϵ_v%
(f)

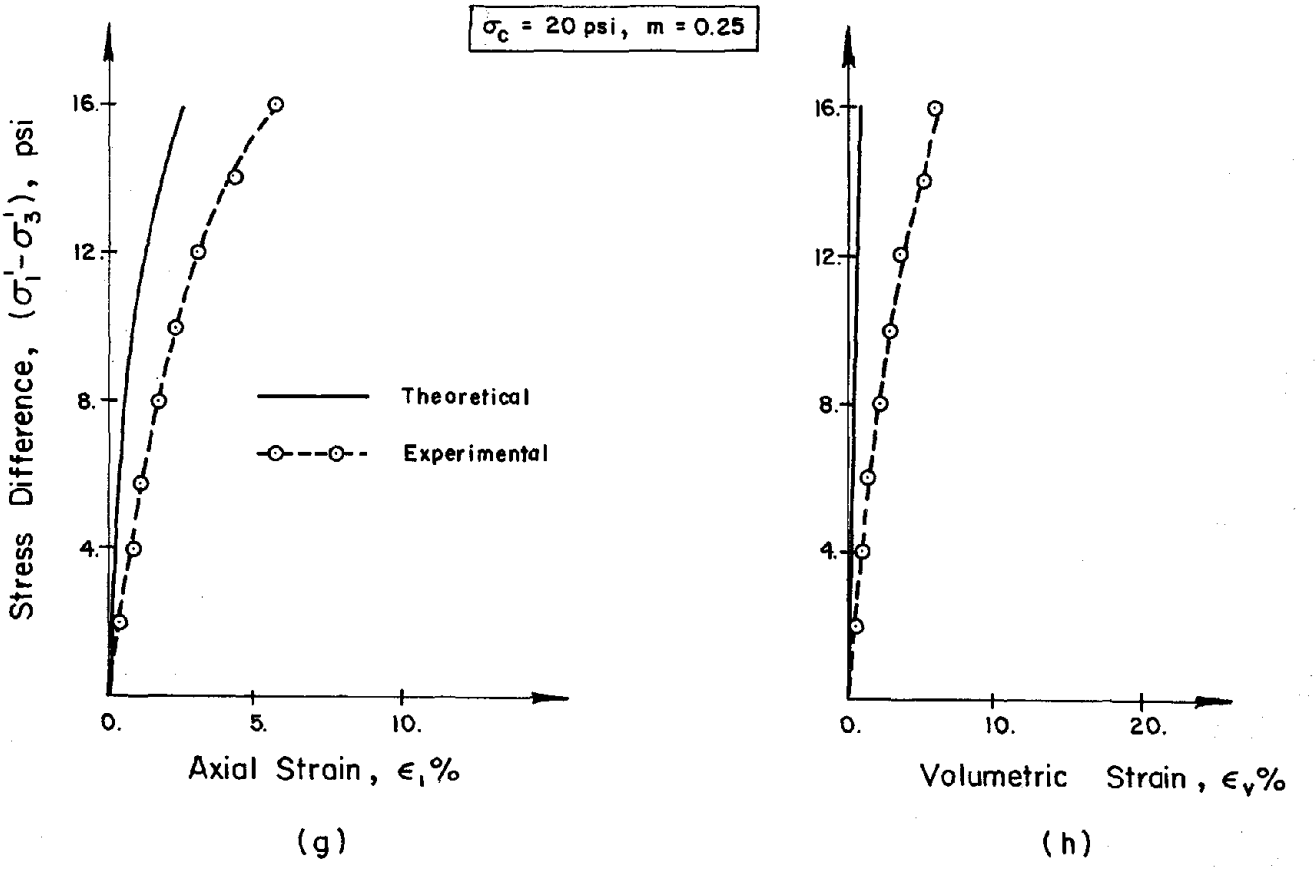
σ_c = 20 psi, m = 0.25
Stress Difference, $(\sigma_1'-\sigma_3')$, psi
16.
12.
8.
4.
Theoretical
Experimental
0.
5.
10.
Axial Strain, ϵ_1%
(g)
16.
12.
8.
4.
0.
10.
20.
Volumetric Strain, ϵ_v%
(h)

FIG 1. (Cont'd)

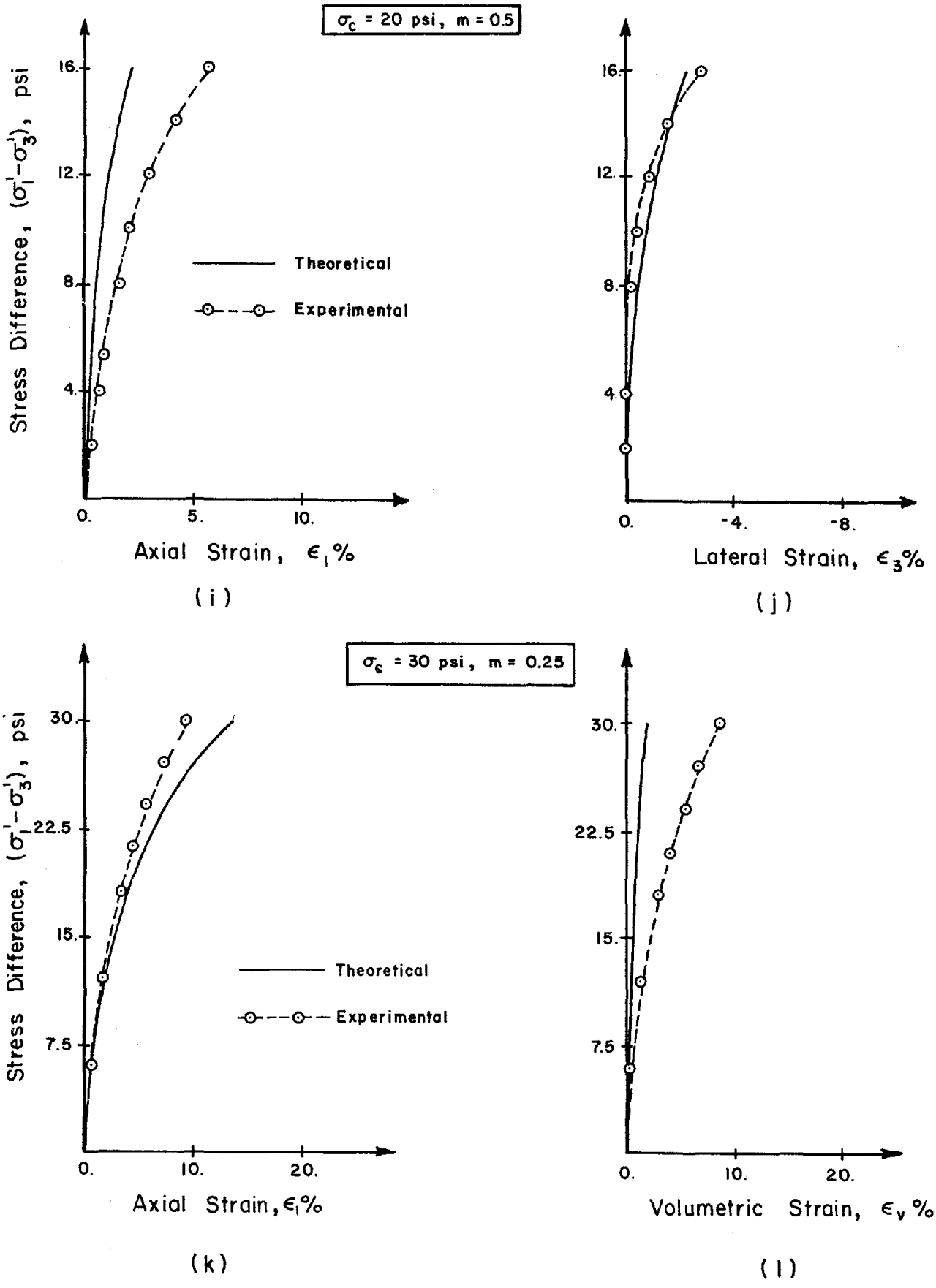
σ_c = 20 psi, m = 0.5
Stress Difference, $(\sigma_1'-\sigma_3')$, psi
16.
12.
8.
4.
0.
5.
10.
Axial Strain, ϵ_1%
Theoretical
Experimental
(i)
16.
12.
8.
4.
0.
-4.
-8.
Lateral Strain, ϵ_3%
(j)
σ_c = 30 psi, m = 0.25
Stress Difference, $(\sigma_1'-\sigma_3')$, psi
30.
22.5
15.
7.5
0.
10.
20.
Axial Strain, ϵ_1%
Theoretical
Experimental
(k)
30.
22.5
15.
7.5
0.
10.
20.
Volumetric Strain, ϵ_v %
(l)

FIG I. (Cont'd)

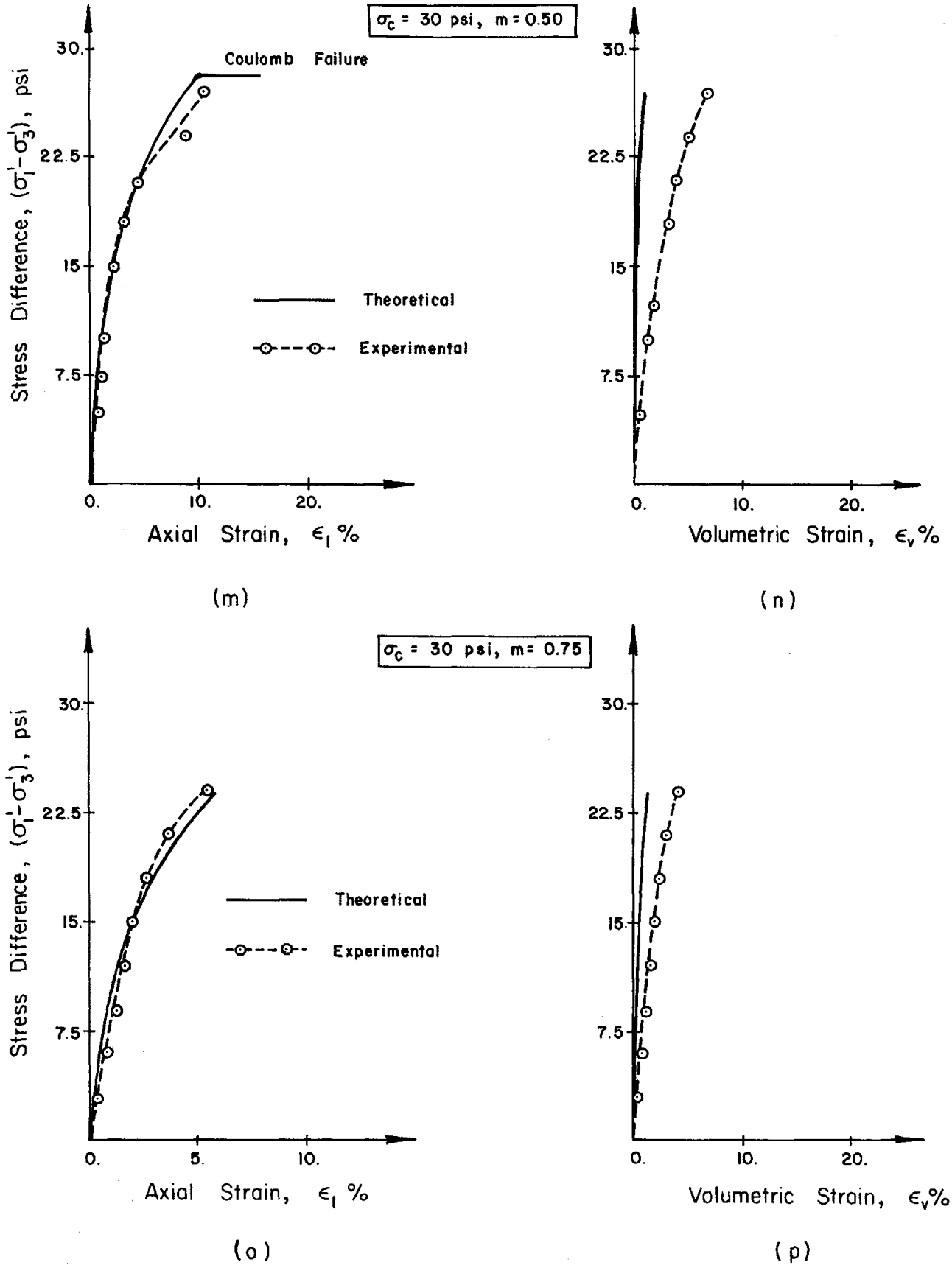
σ_c = 30 psi, m = 0.50
Coulomb Failure
Theoretical
Experimental
Stress Difference, $(\sigma_1'-\sigma_3')$, psi
30.
22.5
15
7.5
0.
10.
20.
Axial Strain, ϵ_1 %
Volumetric Strain, ϵ_v%
(m)
(n)
σ_c = 30 psi, m= 0.75
Theoretical
Experimental
5.
(o)
(p)

FIG 1. (Cont'd)

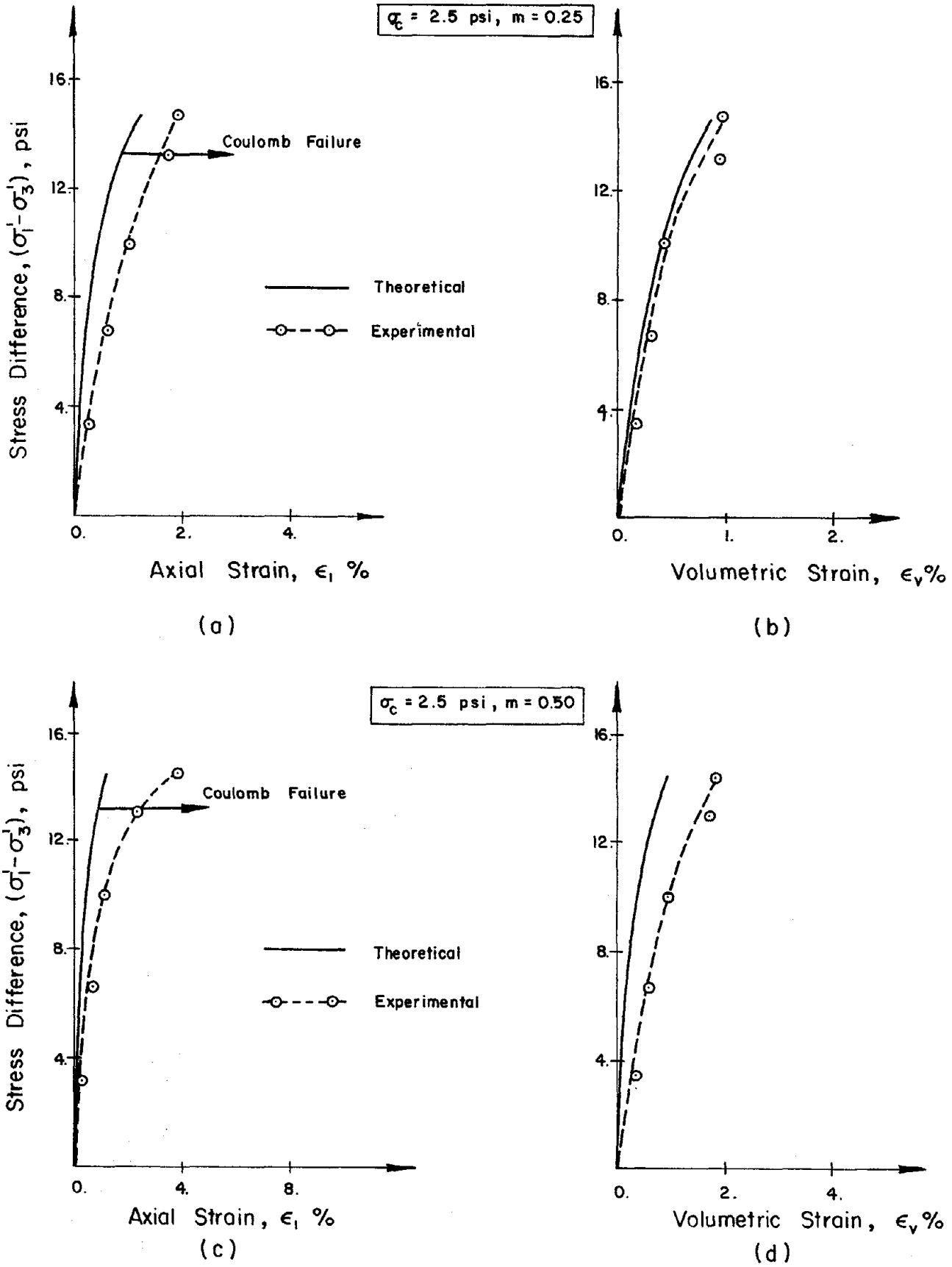

FIG 2. Comparison of the Predicted Theoretical and Experimental Stress-Strain Curves for Clay "Y" (C T C Tests)

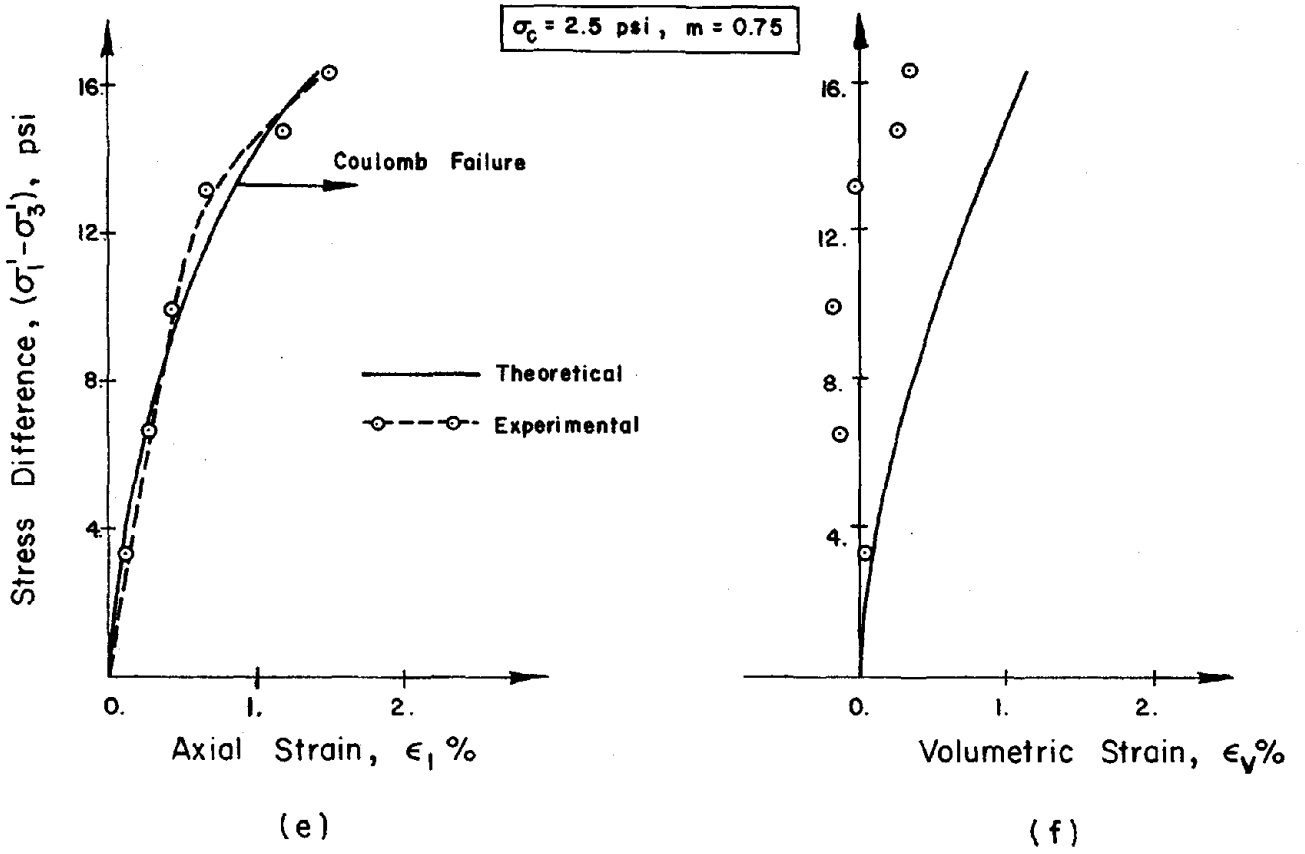
σ_c = 2.5 psi , m = 0.75
Stress Difference, $(\sigma_1'-\sigma_3')$, psi
16.
12.
8.
4.
Coulomb Failure
Theoretical
Experimental
0.
1.
2.
Axial Strain, ϵ_1 %
(e)
16.
12.
8.
4.
0.
1.
2.
Volumetric Strain, ϵ_V%
(f)

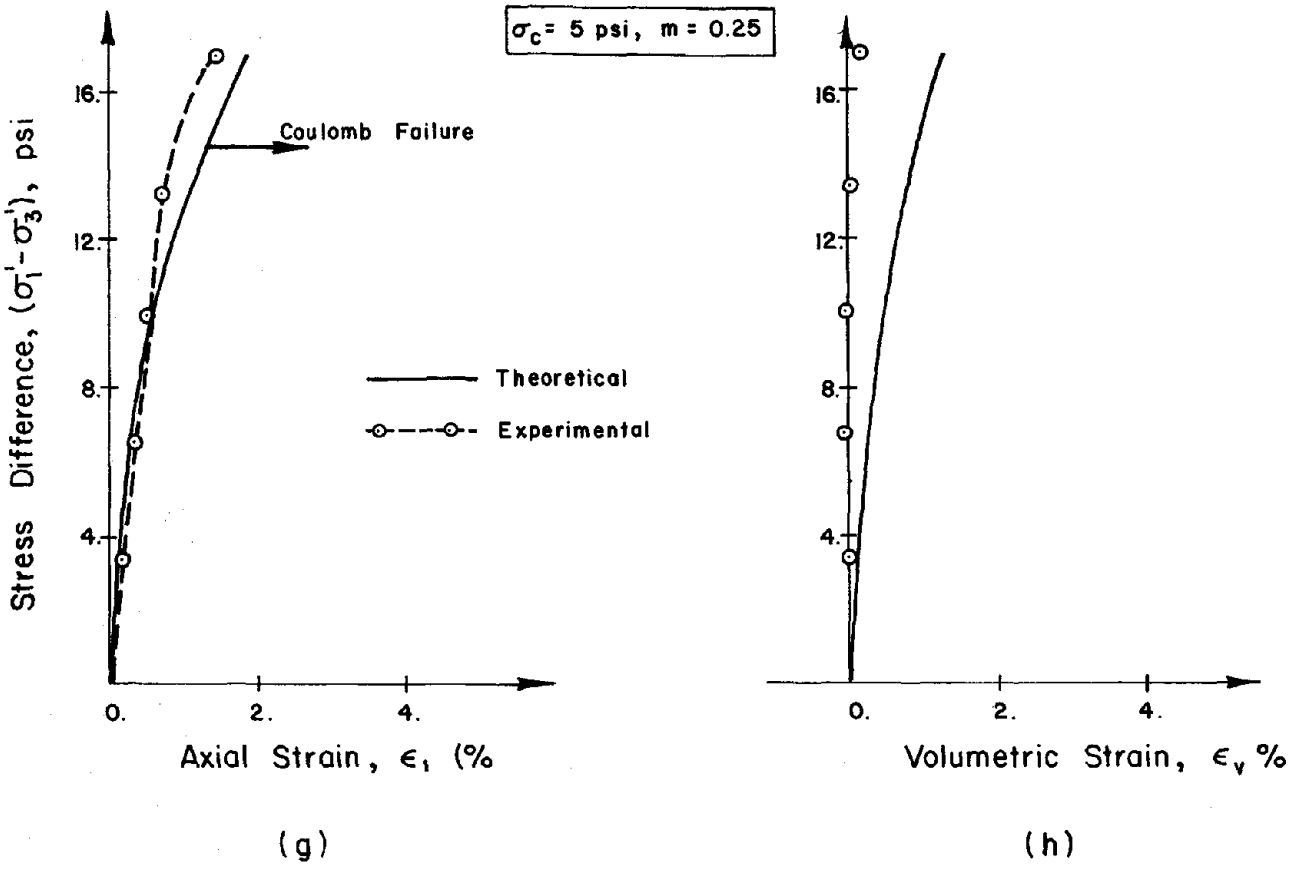
σ_c= 5 psi, m = 0.25
Stress Difference, $(\sigma_1'-\sigma_3')$, psi
16.
12.
8.
4.
Coulomb Failure
Theoretical
Experimental
0.
2.
4.
Axial Strain, ϵ_1 (%
(g)
16.
12.
8.
4.
0.
2.
4.
Volumetric Strain, ϵ_v %
(h)

FIG 2. (Cont'd)

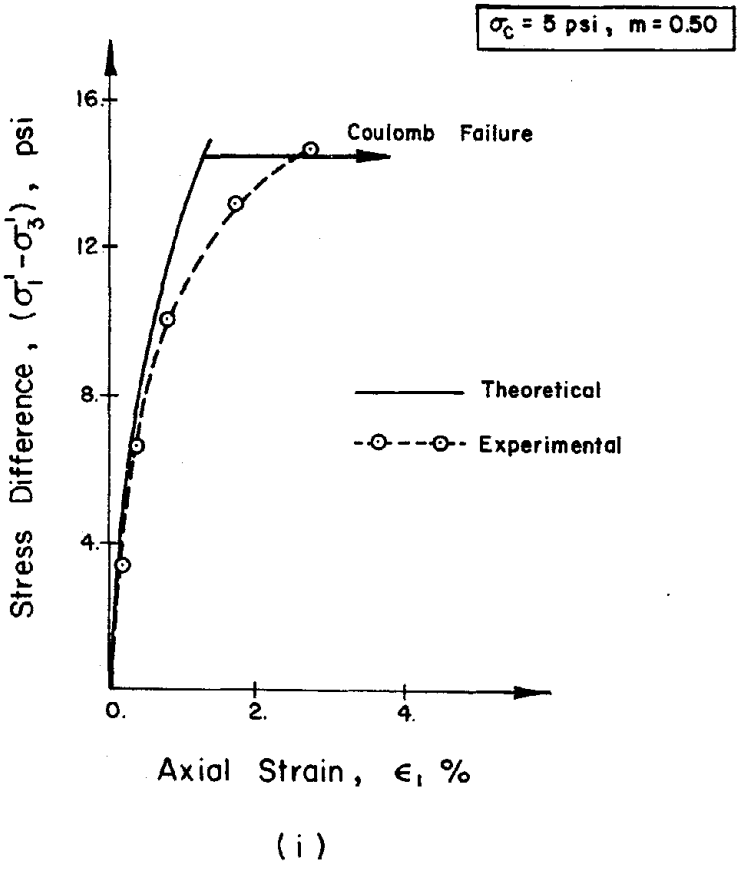

(i)

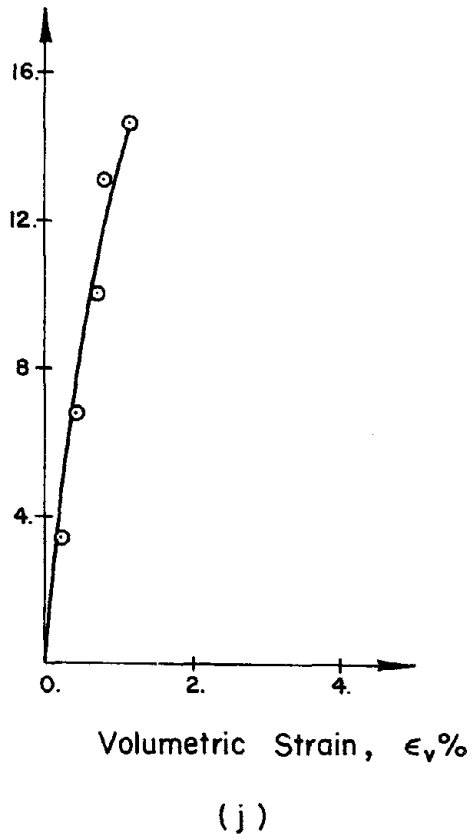

(j)

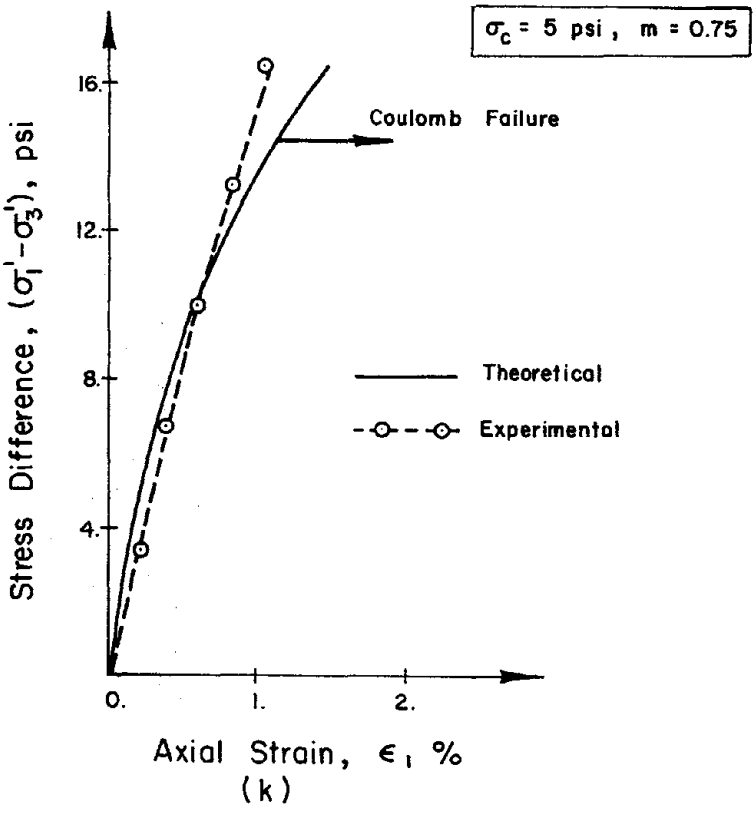

(k)

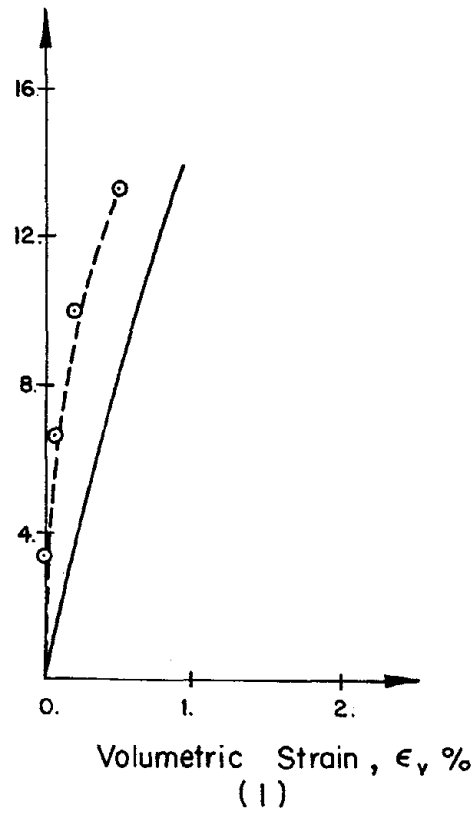

(l)

FIG 2. (Cont'd)

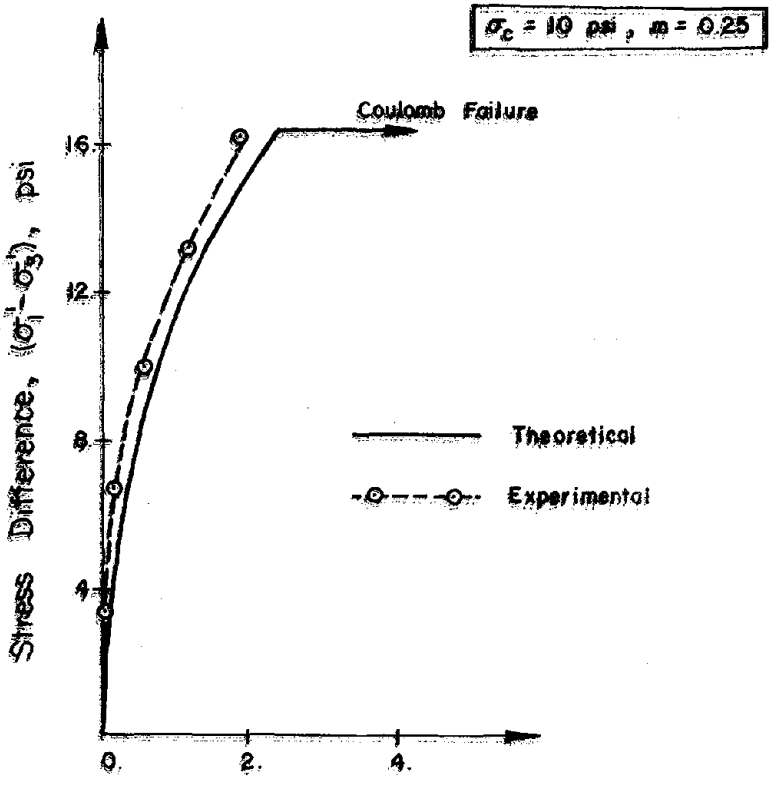

(m)

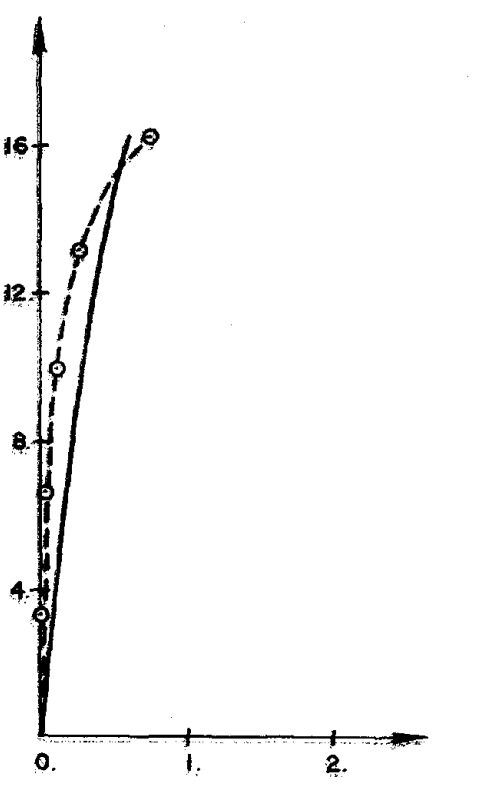

(n)

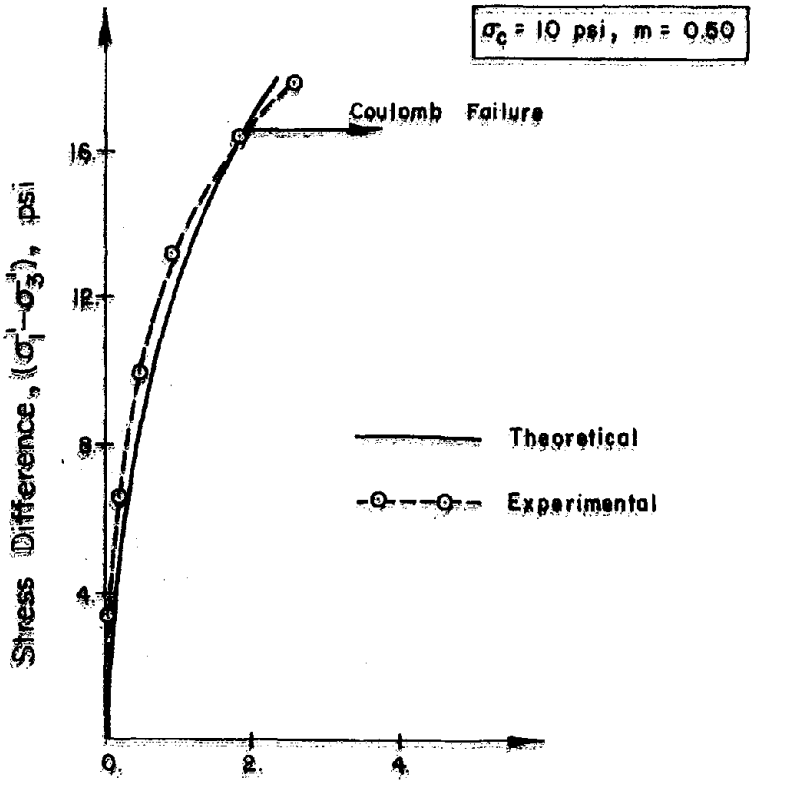

(o)

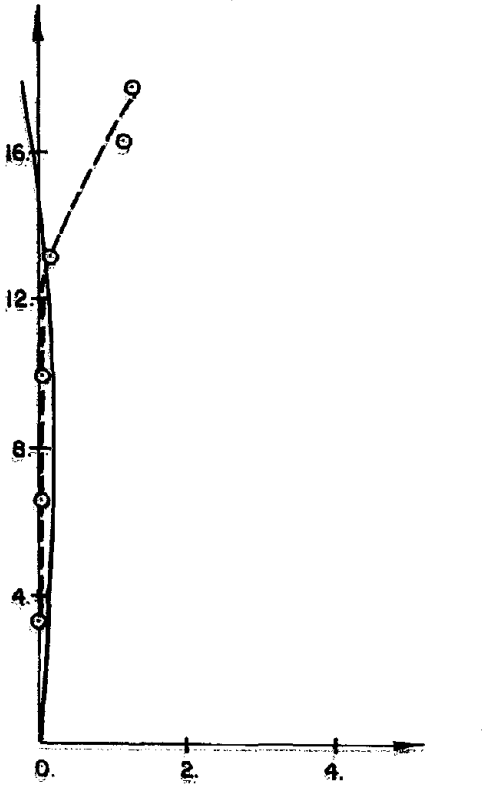

(p)

FIG 2. (Cont'd)

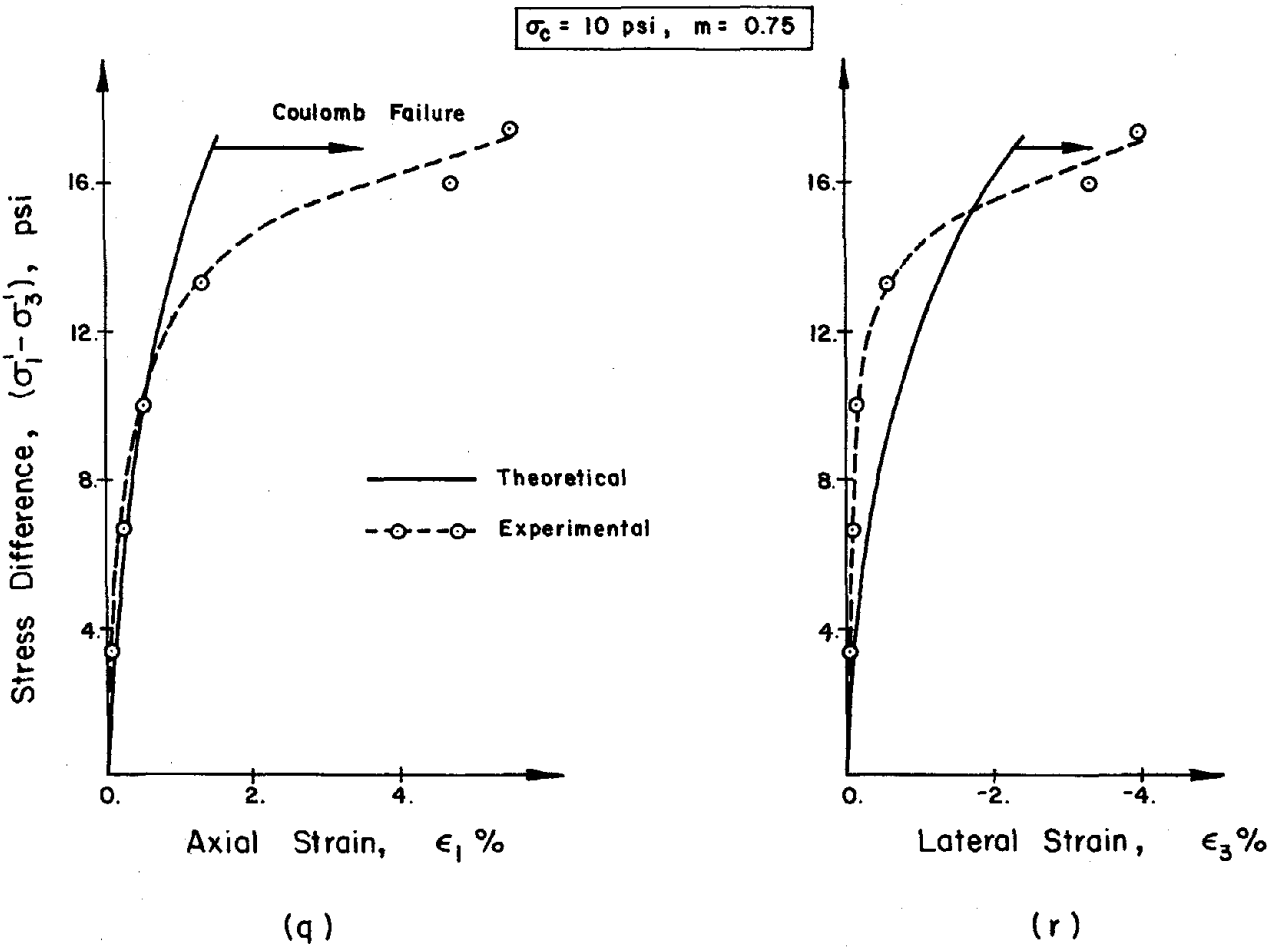
σ_c = 10 psi, m = 0.75
Coulomb Failure
Theoretical
Experimental
Stress Difference, $(\sigma_1' - \sigma_3')$, psi
16.
12.
8.
4.
0.
2.
4.
Axial Strain, ϵ_1 %
(q)
-2.
-4.
Lateral Strain, ϵ_3 %
(r)

FIG 2. (Cont'd)

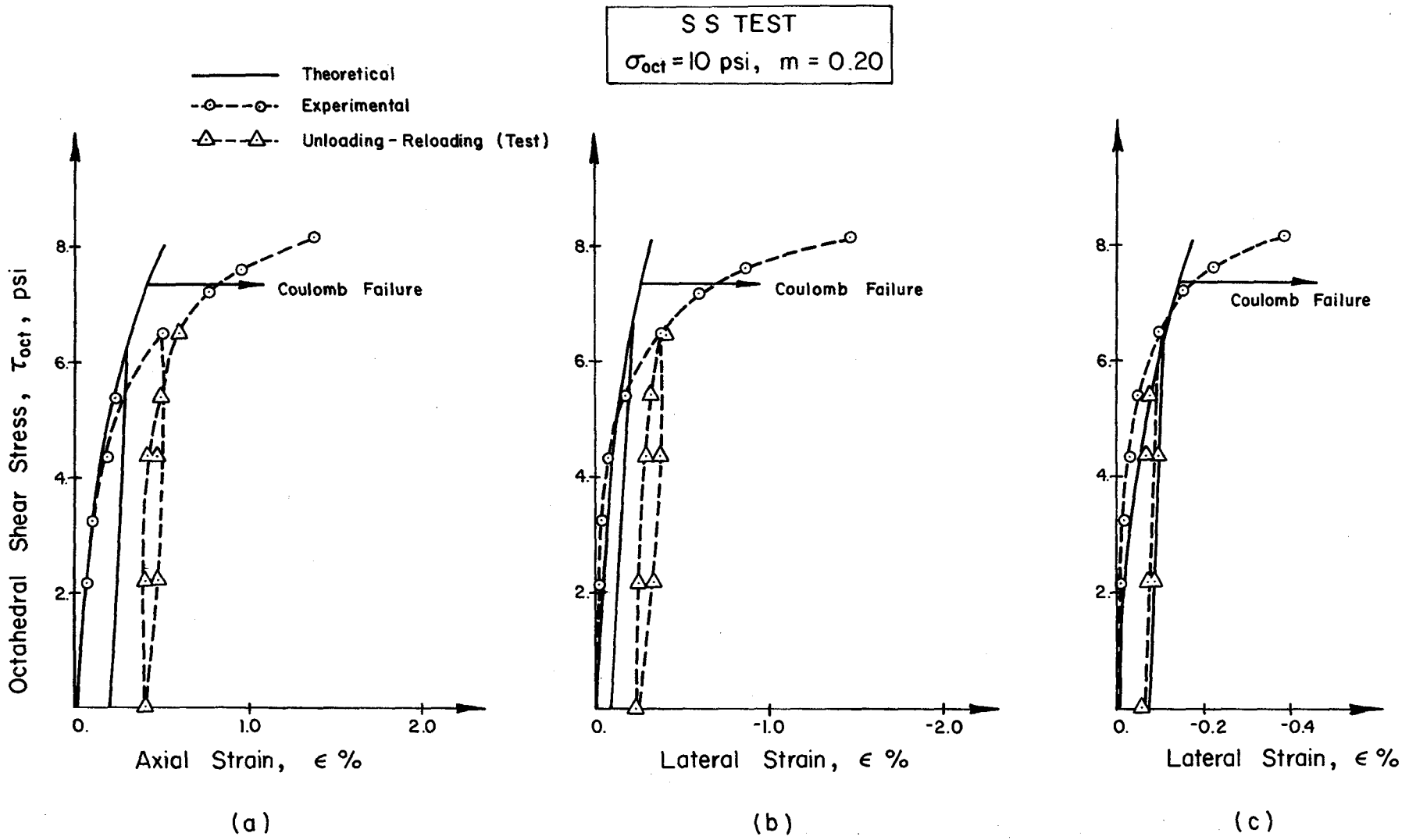

FIG 3. Comparison of the Predicted Theoretical and Experimental Stress-Strain Curves for Ottawa Sand in S S Test (σ_{oct} = 10 psi, m = 0.20)

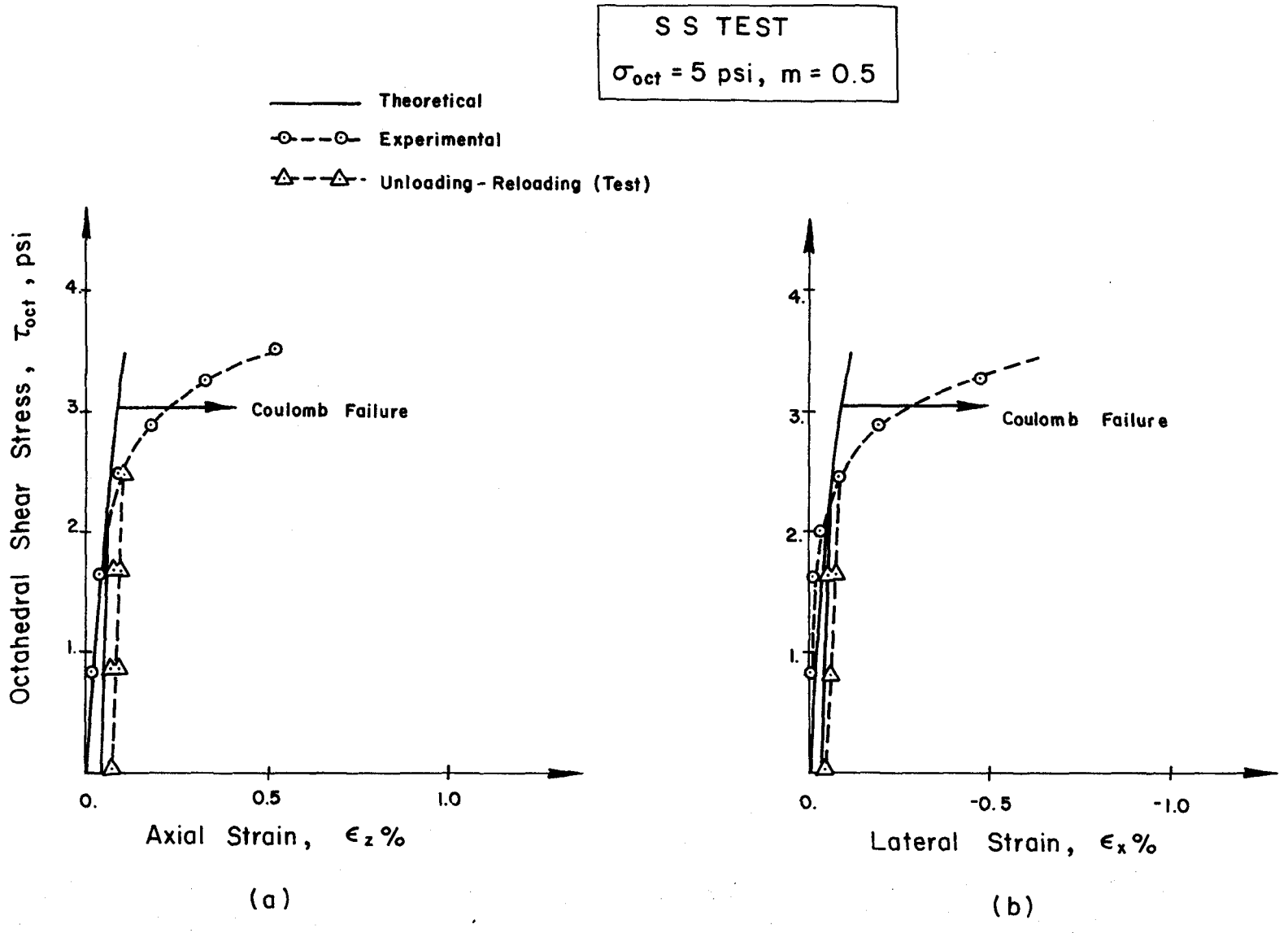

FIG 4. Comparison of the Predicted Theoretical and Experimental Stress-Strain Curves for Ottawa Sand in S S Test (σ_{oct} = 5 psi, m = 0.5)

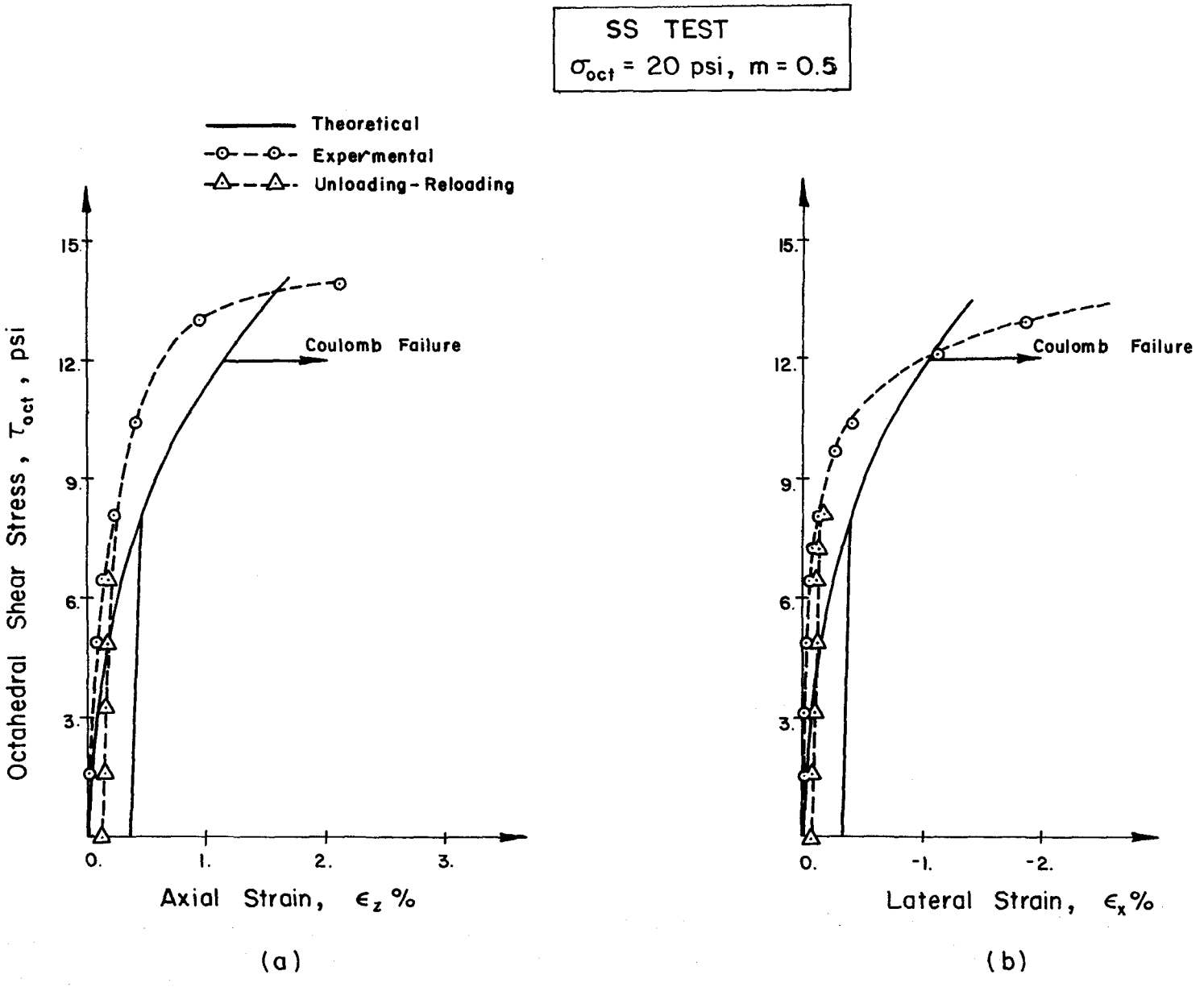

FIG 5. Comparison of the Predicted Theoretical and Experimental Stress-Strain Curves for Ottawa Sand in S S Test (σ_{oct} = 20 psi, m = 0.5)

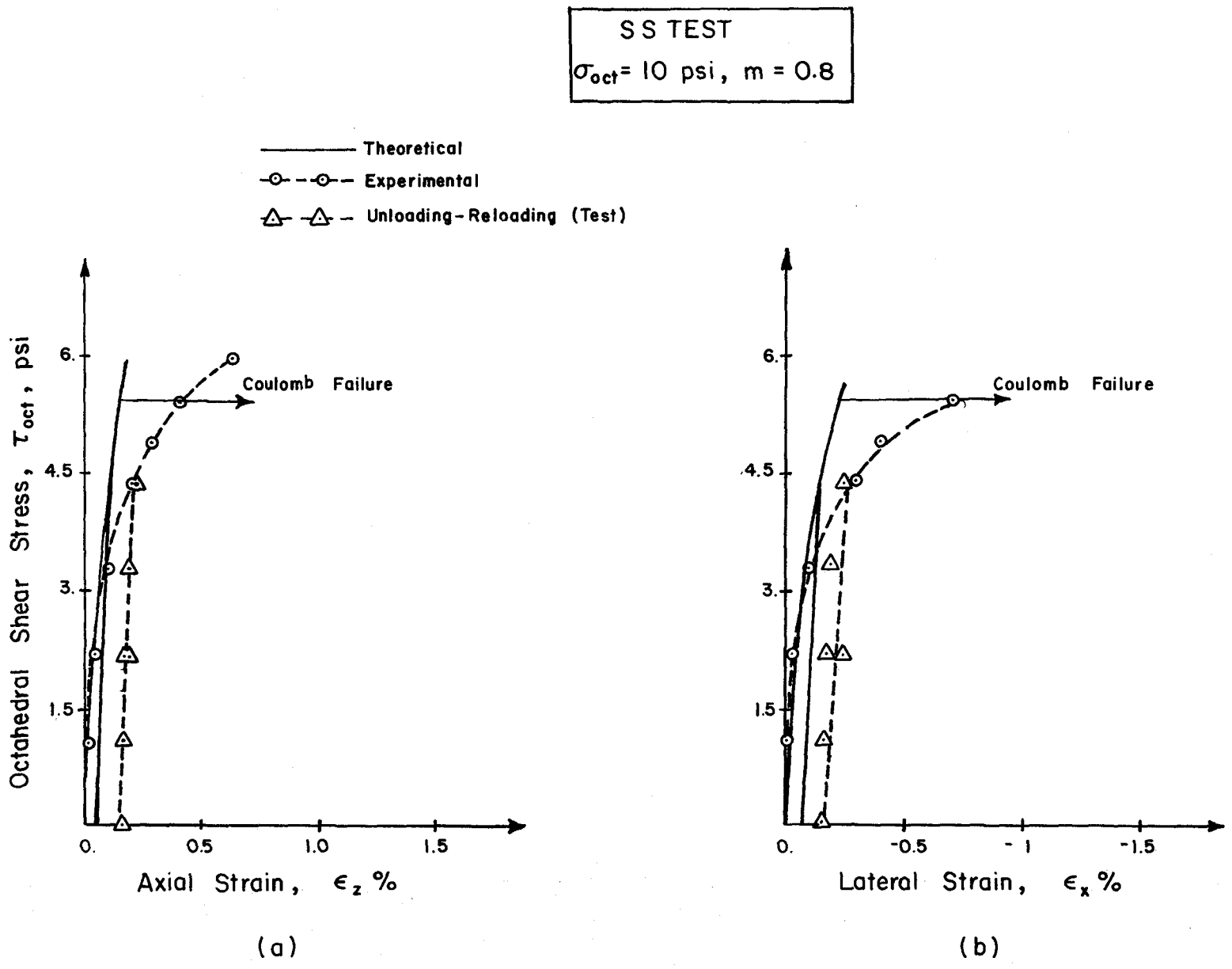

FIG 6. Comparison of the Predicted Theoretical and Experimental Stress-Strain Curve for Ottawa Sand in S S Test (σ_{oct}=10 psi, m= 0.8)

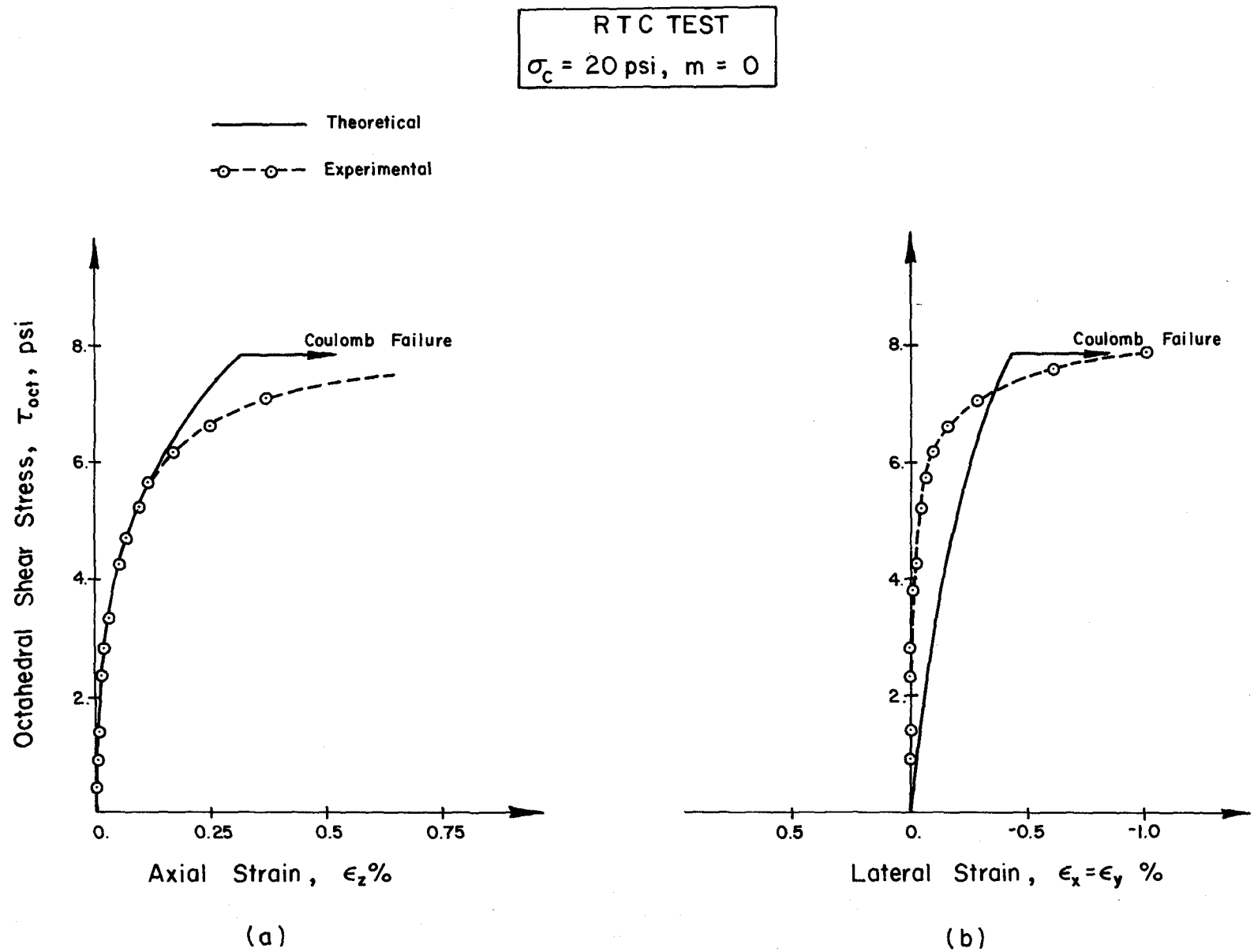

FIG 7. Comparison of the Predicted Theoretical and Experimental Stress-Strain Curves for Ottawa Sand in RTC Test (σ_c = 20 psi, m = 0)

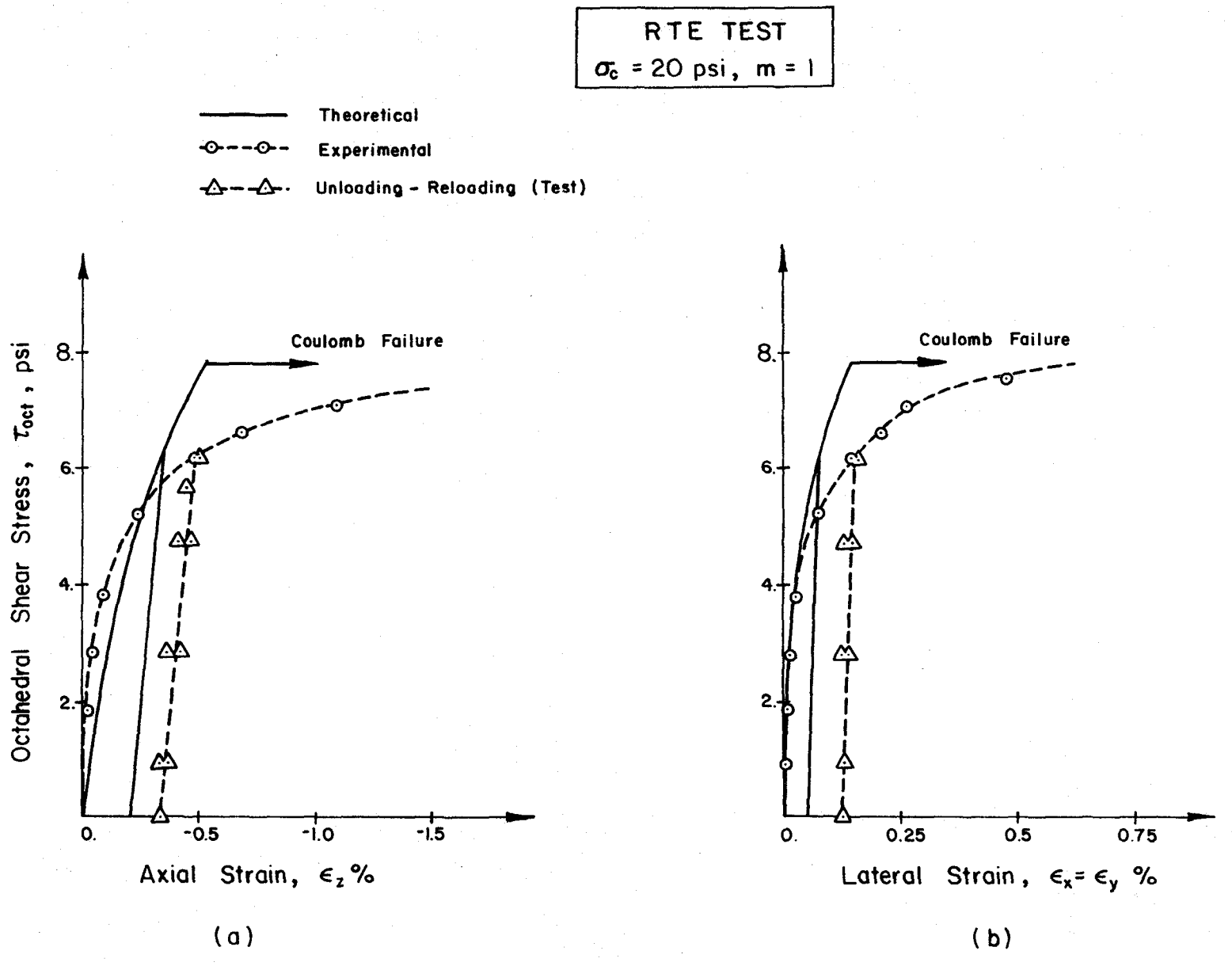

FIG 8. Comparison of the Predicted Theoretical and Experimental Stress-Strain Curves for Ottawa Sand in RTE Test (σ_c = 20 psi, m = 1).